CHAPTER 3 : THE ORIFICE FLOW OF SEMI-RIGID POLYMER SOLUTIONS.

Abstract

The orifice flow of scleroglucane solutions is studied. Under given conditions of temperature and solvent quality, this molecule behaves as a semi-rigid rod in solutions.

Solutions in glucose-water syrups may show considerable vortex growth in orifice flow depending on flow regime and concentration. The vortex reattachment length and the slope of the vortex boundary are studied as a function of regime and concentration.

The flow curves in orifice flow are characterised by a linear P_g - q_v relation. The extensional viscosity is derived from the orifice flow data by the Binding analysis. Comparison with the Batchelor analysis for closely spaced fibers is satisfactory if molecular extension as well as alignment along the streamlines is considered.

3.1. Introduction.

Having studied in the previous chapter the influence of the concentration on the behavior of flexible polymer solutions in contraction flows, we shall be interested here in the behavior of semi-rigid chain polymer solutions in the same flow.

Rigid polymer solutions are believed to be in general much less elastic than flexible ones. Barnes et al [1] illustrate this by a spectacular phenomenon produced in a complex two dimensional flow made up of wide and narrow channels. When a Newtonian fluid is flowing in this geometry, a certain quantity is passing through the narrow channels. In the case of a flow of an inelastic xanthan gum solution in the same geometry substantially higher quantities find their way through the narrow channels, due to important shear thinning. On the contrary, with a highly elastic polyacrylamide solution, the inverse phenomenon is observed: no fluid finds its way though the narrow channels because extensional viscosity considerations become most important.

In the same reference, viscometric data is given for xanthan gum solutions. These solutions are highly shear-thinning, but their extensional viscosity takes much smaller values than these of similar concentration flexible polymer solutions.

Solutions of rigid polymers are expected to behave like suspensions of rigid slender particles. For the latter, constitutive equations are available in the dilute range [Hinch and Leal, 10-12]. The interesting range of semi-dilute systems has been examined by Batchelor [3] for elongationnal flows. Different extensions based on the

micromechanics of ellipsoidal particles have been proposed by Dinh and Armstrong [9] and Lipscomb et al [5].

Many authors have been interested in the experimental flow properties of rigid slender particle solutions. Mewis and Metzner [2] studied solutions of glass fibers of aspect ratio varying from 280 to 1260 in a low molecular weight polybutene. The extensional viscosity measured by the spinneret method was found to obtain values as high as 260 times the zero shear viscosity of the suspending fluid. Their results verified the analysis of Batchelor concerning semi-dilute suspensions of closely spaced slender particles [3].

More recently, attention was given also to contraction flows of such systems. Binnington and Boger [4] showed that vortices exist upstream of a contraction in the flow of suspensions of fibers of glass and solutions of xanthan gum in a corn syrup. They found almost constant vortex length throughout the range of regimes examined (2 to 40 s^{-1}). They thus stressed the point that for macro as well as for micro semi-rigid rod systems, extensional viscosity should be certainly higher than that of the solvent, but almost independent of the extensional rate. Furthermore, their first normal stress difference varies linearly with shear rate, which establishes them as an important subgroup of constant viscosity elastic fluids.

Lipscomb et al. [5] developed a theory incorporating the statistical orientation distribution function into the stress equation. Based on this constitutive equation, they developed a numerical model for the contraction flow under inertialess conditions. A key assumption in this model is that fibers are aligned with streamlines. Numerical simulation results were compared to experiments with glass fibers suspended in a viscous syrup (Length of fibers : 3 and 6mm. Aspect ratios respectively 276 and 552). Good agreement was observed for the flow field structure and the variation of the reduced vortex reattachment length X with the different parameters : X increases considerably with fiber concentration for a given aspect ratio. Analysis of the published data also shows that X increases with aspect ratio at given volume concentration. The vortex length was also found to be independent of the Reynolds number, and to increase slightly with the contraction ratio.

Chiba et al [6] presented numerical results which agreed with those of Lipscomb et al, and extended them by considering the effect of inertia. Concentration was again shown to increase the vortex length and inertia to crush the vortices. It was also supposed that the length of the vortex is independent of the flow rate when fibers of polymer molecules do not change their configuration.

In another numerical study, Keiller et al [7] examined more generally sink flows of suspensions of rigid rods. They established the way vortex enhancement varies with concentration. On the other hand, Keiller and Hinch in their analysis [8], find that the vortices should indeed exist, but decrease with concentration. Their analysis is valid

only in a very small neighborhood of the corner, as the rods must experience the flow for long enough to adopt the de-aligned orientation. They suggested therefore that the vortices observed by the previously mentioned authors are a consequence of the contraction flow and not the flow singularity.

Vugmeister et al [13] examined aqueous suspensions of monodisperse rigid PTFE rods of very low aspect ratio (2.5). The orientational order parameter was measured during shear flow versus the shear rate. A strong concentration dependence was observed and the drastic enhancement of the orientational parameter happened at a volume fraction of 38 %.

The above studies show that flow induced orientation of slender rigid bodies may generate considerable elongationnal effects. In contraction flows this results in viscoelastic vortices, that seem to be flow rate independent in the regimes examined. It should be expected that other flow regimes might exist at lower flow regime conditions : at very low flow rates where particle orientation should be random, the fluid is Newtonian, and contraction flow should resemble to that of a newtonian fluid, with concave corner vortices. The evolution from the Newtonian corner vortices to the flow rate independent viscoelastic vortices has not been studied yet. Another aspects that worths further investigation is the effect of elongationnal properties of slender rigid particle suspensions on the excess pressure drop in the contraction flow.

In the present chapter, we present orifice flow experiments with solutions of scleroglucane, a semi-rigid chain polymer, in a thick solvent. The objective is to study elongationnal effects generated in this geometry and to confront observations with predictions on the elongationnal viscosity from slender rigid body theories and orifice flow analysis.

In section 3.2 we describe the polymer as well as the method of the preparation of fluids of different concentrations. The shear viscosity of these fluids is given in section 3.3. Section 3.4 treats the orifice flow of these solutions and the instabilities observed in this flow. Unlike former studies, regimes with considerable vortex growth are observed. The extensional viscosity is discussed in section 3.5, derived from the orifice flow data and independent model predictions. The conclusion is given in 3.6.

3.2. Working fluids.

3.2.1. The polymer.

The fluids considered in this section are solutions of scleroglucane, which is a semi-rigid chain polymer. It is a polysaccharide similar to xanthan and in our case it

was provided by Elf Sanofi in powder form. It has a molecular weight of about 5.10^6. It is used in the oil industry and is soluble in water.

The scleroglucan is a microbial polysaccharide. Its chemical repeating unit is :

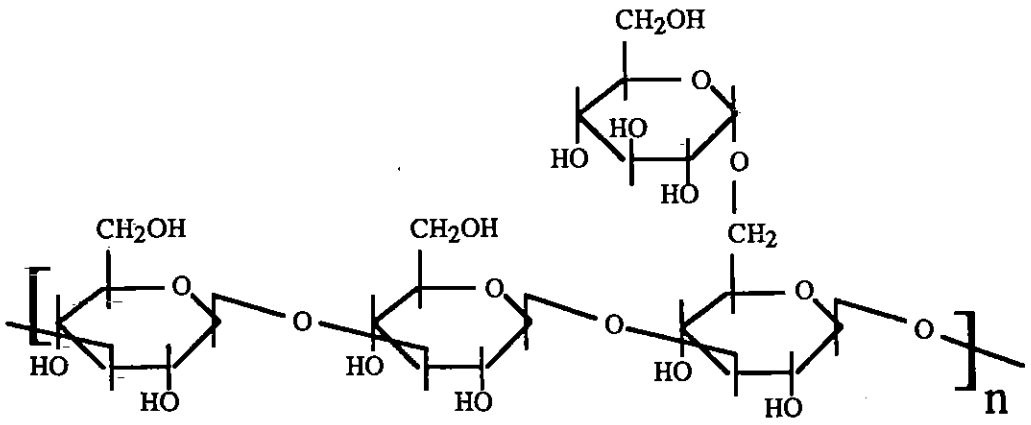

similar to schizophylan, another microbial saccharide which has a different biological origin.

Nardin and Vincendon [21] have examined the conformation of scleroglucan by measuring the isotopic exchange OH/DO in solutions in D_2O, which shows the degree of accessibility of the hydroxyls and thus, the degree of the molecule's structure. They showed a triple helical structure. Increasing the temperature as well as adding lithium chloride resulted in a continuous disorder effect which facilitated accessibility to D_2O. They have also shown that, when dissolved in DMSO, the molecule is dispersed to take up a single-chain random-coil conformation.

Yanaki et al [20], using light scattering, viscometry and chemical analyses found that its intrinsic viscosity is 243 cm^3g^{-1} in DMSO (flexible chain), but in 0.01N NaOH it obtains much higher values ($6.6.10^3$ cm^3g^{-1}) since it is rodlike. Yanaki and Norisuye [19] found in the latter solvent and at 25°C a contour length per main chain residue of h= 0.3 nm, a diameter of trimmer rod of 2.5 nm and an intrinsic viscosity of 4.4 10^3 cm^3g^{-1}.

Itou et al [22] achieved optical rotation and heat capacity measurements on aqueous solutions of schizophyllan. They showed a sharp transition at about 6°C : an order-disorder transition in a relatively short range surrounding its triple-helix, resulted in changes in the heat capacity, in the optical rotation and in the intrinsic viscosity. The latter passed from 269 to 265 cm^3g^{-1} within some degrees centigrade, though it has been constant for lower and higher temperatures.

Noik and Lecourtier [23] found an intrinsic viscosity of 9200 cm^3g^{-1} and a Huggins constant of k'= 0.5 at 30°C for aqueous solutions.

The above-mentioned literature data on the intrinsic viscosity of scleroglucane indicate that in a solution, it can behave either as a rigid polymer with a triple-helix

structure or as a flexible polymer, depending on the solvent as well as on the temperature. At room temperatures and for a molecular weight close to ours (about $5 \cdot 10^6$), its intrinsic viscosity may vary from 240 cm^3g^{-1} (as flexible polymer) up to 10^4 cm^3g^{-1} (as a rigid polymer).

3.2.2. Preparation of the solutions.

Solutions of this polymer were prepared in a glucose/water syrup, as well as in water. Two aqueous solutions were prepared (concentrations of 0.1% and 1% w/w), by simply dissolving the polymer powder in the appropriate demineralised water quantity, and letting it agitate with an impeller agitator during 10 hours.

As it was soon realized, these aqueous solutions are strongly shear-thinning, and the orifice flow of these solutions would be governed by shear-thinning and inertial phenomena even at very low regimes. Thus, glucose/water syrups were used as solvents.

Solutions of concentrations of 100, 500 and 5000 ppm (w/w) were prepared in a solvent of 80/20 glucose/water as well as a solution of 2000 ppm in a thicker syrup (90/10)(see table 3.1). Polymer was first dissolved progressively in demineralised water and stirred with the help of an impeller agitator for about 5 hours. The resulting fluid was stored for 24 hours and was again stirred in a magnetic agitator for 1 hour. It was then gradually poured to glucose, stirred manually for about 1 hour, and let to agitate during 5 days to ensure homogeneity.

The solutions of concentration higher than 500 ppm were found hard to produce with the same procedure, because homogeneity was difficult to obtain for these concentrations in the original aqueous fluid as well as in the glucose mixture. Thus, an excessive water quantity was initially used, which was let to evaporate during the final agitation with the glucose, by controlling the total weight. Thus the preparation time for the 2000 and 5000 ppm solutions was several days.

All solutions were protected against bacterial degradation by adding 400 ppm by weight NaN_3.

3.3. The shear viscosity measurements.

3.3.1. The aqueous solutions.

The shear viscosity of the scleroglucane solutions has been measured by the CarriMed Controlled Stress Rheometer and controlled for each new sample produced. A

cone-plate geometry has been used with a cone angle of 1° and a diameter of 6 cm. All measurements were carried out at a temperature of 20°C.

With the flow experiment technique at shear gradients as low as 10^{-2} s^{-1} we were not able to reach the initial Newtonian plateau for both aqueous solutions, and thus, the creeping flow technique has been applied (Annex A). At shear rates of the order of 10^{-4} s^{-1} and even lower the Newtonian plateau is not yet reached, even though shear-thinning becomes much less important (Fig. 3.1). The form of the curves indicates a zero shear viscosity value of about η_0= 50 Pas for the 0.1% solution and of about $\eta_0 = 8 \cdot 10^3$ Pas for the 1%. For the later, this gives a zero-shear viscosity about 10^7 times that of the solvent (we remind that the viscosity of water is 10^{-3} Pas at 20°C). In the strong shear-thinning region (10^{-2} $s^{-1} < \dot{\gamma} < 10^2$ s^{-1}), the 0.1% behaves as a power law fluid with n= 0.28. The slope of $\log(\eta(\dot{\gamma}))$ versus $\log\dot{\gamma}$ diminishes considerably for $\dot{\gamma} > 10^{-2}$ s^{-1} (n= 0.69) and at $\dot{\gamma} = 25 \cdot 10^2$ s^{-1} the viscosity attains $3 \cdot 10^{-3}$ Pas, a value only 3 times that of the solvent. No information is available beyond this value.

Shear-thinning is even more important with the 1% solution. In the power law region, which covers more than six decades (10^{-3} $s^{-1} < \dot{\gamma} < 2 \cdot 10^3$ s^{-1}), it is n= 0.14. At $\dot{\gamma} = 25 \cdot 10^2$ s^{-1} it attains $\eta = 25 \cdot 10^{-3}$ Pas.

3.3.2. The glucose syrup solutions.

The same geometry was used to measure the shear viscosity of the solutions in the glucose/water syrup which is shown in Fig. 3.2.

No shear-thinning was detected for the 100 ppm solution within the precision of the instrument. Its constant shear viscosity at 20°C is η= 1.27 Pas. Slight shear-thinning can be observed for the 500 ppm solution. For $\dot{\gamma} > 1 s^{-1}$ it behaves as a power-law fluid with n= 0.97. Its zero shear viscosity is 1.85 Pas, attained for $\dot{\gamma} < 1 s^{-1}$.

The 2000 and 5000 ppm solutions are more shear-thinning (n= 0.935 and 0.83 respectively). As the content in glucose is higher in the 2000 ppm fluid, this later has a higher viscosity from the 5000 ppm one. Their zero-shear viscosities were achieved for shear gradients lower than 5.10^{-2} s^{-1} and they are 19.5 and 15.5 Pas respectively.

In the power law region the following equations match perfectly the data:

$$500 \text{ ppm}: \quad \eta = 1.85\dot{\gamma}^{-0.03} \quad (\text{for } 1 s^{-1} < \dot{\gamma} < 100 s^{-1}) \tag{3.1}$$

$$2000 \text{ ppm}: \quad \eta = 13.68\dot{\gamma}^{-0.065} \quad (\text{for } 5.10^{-2} s^{-1} < \dot{\gamma} < 10 s^{-1}) \tag{3.2}$$

$$5000 \text{ ppm}: \quad \eta = 8.0\dot{\gamma}^{-0.17} \quad (\text{for } 5.10^{-2} s^{-1} < \dot{\gamma} < 30 s^{-1}) \tag{3.3}$$

These power relationships were valid till the highest shear gradient attained within the limitations of the geometry used.

In Fig. 3.3 we compare the relative viscosity: $\frac{\eta_0(c)}{\eta(0)}$ of the scleroglucane solutions with this of the PEO solutions (chapter 2). For the same concentration, the relative viscosity is higher than with PEO, which is not surprising if one considers scleroglucan's higher molecular weight.

The intrinsic viscosity and the Huggins coefficient (eq. 2.9 and 2.10) are estimated to be: $[\eta_0] = 580\ cm^3g^{-1}$ and $k' = 0.73$. As previously mentioned, values of several thousands (6 to $9 \cdot 10^3\ cm^3g^{-1}$) have been reported for the intrinsic viscosity of this polymer, in the conditions where it has a triple helical (rigid) structure. On the contrary, much lower values (about $250\ cm^3g^{-1}$) have been reported in the case where it behaves like a flexible polymer (for example in DMSO). In our case, the value of $580\ cm^3g^{-1}$ indicates an intermediate situation. This point will be further discussed at the end of section 3.3.3.

The following table reports the shear data of the solutions:

Table 3.1. η_0 and λ values of the scleroglucane glucose syrup solutions at 20°C.

c (ppm)	gluc.(%)	η_0 (Pas)	η_s (Pas)	c_v (g/l)	λ (sec)
100	80	1.3	1.2	0.136	0.032
500	80	1.9	1.2	0.68	0.823
2000	90	19.5	5.0	3.0	101.6
5000	80	15.5	1.2	6.8	79.6

where η_s is the solvent viscosity, c_v the volume concentration and λ the characteristic time evaluated in such a way in order to correspond to the rotational relaxation time. The calculation of this time scale is described in detail in the following.

We plotted the specific viscosity versus the reduced concentration $[\eta_0]\, c_v$ (Fig. 3.4). The term of first order of the equation:

$$\eta_{sp} = \eta_{rel} - 1 = \frac{\eta - \eta_s}{\eta_s} = [\eta_0]\ c_v + k'[\eta_0]^2 c_v^2 \qquad (3.4)$$

is sufficient to describe the specific viscosity of the 100 ppm solution, while for the 2000 and 5000 ppm solutions the second order term is necessary. The 500 ppm does not deviate a lot from the first order equation.

The classification of the solutions in concentration regimes is discussed in the following.

3.3.3. Concentration regimes.

Doi and Edwards [25] classify the solutions of rodlike polymers into four concentration regimes. Denoting by L the length of the rods, b their diameter, c_v the weight per volume concentration and n the number of polymers per unit volume :

$$n = c_v \frac{N_A}{M} \qquad (3.5)$$

the classification of Doi and Edwards is :

• Dilute solutions, where the concentration is sufficiently low for the average distance between the polymers to be much larger than L. In such a solution each polymer can rotate freely without interference by other polymers. Considering the upper limit of this concentration regime n_1, the condition is :

$$n < n_1 = L^{-3} \qquad (3.6)$$

• Semi-dilute solutions, where :

$$\frac{1}{b\,L^2} = n_2 >> n \geq n_1 \qquad (3.7)$$

The rotation of each polymer is here severely restricted by other polymers, so that the dynamics of the polymers will be entirely different from that in dilute solution. The static properties are though not seriously affected until the concentration reaches n_2.

• Concentrated solutions :

$$n^* > n \geq n_2 \qquad (3.8)$$

In this concentration regime, polymers tend to orient in the same direction as their neighbours. The excluded volume interactions among the polymers are important in both the static and the dynamic properties.

• Liquid crystalline solutions : $n > n^*$. The critical concentration n^* is in the order of n_2. In this regime the polymers align on a macroscopic scale in equilibrium, and the solution becomes an anisotropic liquid.

Transitions from one regime to another are smooth, so n_1, n_2 and n^* are indicative values for progressive changes in the solution properties.

In the dilute range, the intrinsic viscosity is given by [25]:

$$[\eta] = \frac{2\pi L^3}{45\left(\ln\left(\frac{L}{b}\right) - \gamma\right)} \frac{N_A}{M} \qquad (3.9)$$

where N_A is the Avogadro number and γ=0.8 is a correction factor. The rotational relaxation time for dilute solutions is :

$$\lambda_{r0} = \frac{1}{2 D_r} = \frac{\pi \eta_s L^3}{6\left(\ln\left(\frac{L}{b}\right) - \gamma\right) k_B T} \qquad (3.10)$$

where k_B is the Boltzmann constant and D_r is the rotational diffusion constant.

For semi-dilute solutions, the rotational relaxation time is larger than in dilute solutions by a factor :

$$\frac{\lambda_r}{\lambda_{r0}} = \frac{(n L^3)^2}{\beta} \qquad (3.11)$$

where β is a correction factor of the order of 10^3.

In the case of our scleroglucane solutions, the diameter is close to 3nm [19, 23]. From the calculated intrinsic viscosity (eq.3.9) we find L= 0.53 µm and L/b= 180. The limits of the concentration ranges are then :

$$n_1 = 6.72\ \mu m^{-3} \quad \text{and} \quad n_2 = 1210\ \mu m^{-3}$$

For our lowest and highest concentration solutions the correspondance may be written as:

$$c = 100\ ppm \Rightarrow n = 16.4\ \mu m^{-3} \quad \text{and} \quad c = 5000\ ppm \Rightarrow n = 820\ \mu m^{-3}$$

which indicates that the whole range of our solutions is situated in the semi-dilute range.

The calculation of the relaxation time of the solutions is shown in table 3.2.

Table 3.2. Relaxation time of the scleroglucane glucose syrup solutions.

c (ppm)	gluc.(%)	λ_{T0} (sec)	$n L^3$	λ_T or λ (sec)
100	80	5.35	2.44	0.032
500	80	5.35	12.2	0.823
2000	90	42.65	48.8	101.6
5000	80	5.35	122.0	79.6

The reduced shear viscosity was then plotted versus the reduced shear gradient (Fig. 3.5). The onset of shear-thinning occurs at $\lambda\dot{\gamma} \cong 1$. It is also observed that shear-thinning becomes more pronounced as concentration is increased. This was also observed for the PEO solutions in Chapter 2.

Discussion

The $[\eta]$ value obtained in this study is based on the viscosity values of the 100 and 500 ppm solutions at zero shear rate. The error in the viscosity measurements is about 5%. This gives :

for the solvent	η = 1.2 +/- 0.06 Pas
for the 100ppm solution	η = 1.3 +/- 0.07 Pas
for the 500ppm solution	η = 1.9 +/- 0.10 Pas

and so :

for the 100ppm solution	$\eta_0 - \eta_s$ = 0.1 +/- 0.1 Pas
for the 500ppm solution	$\eta_0 - \eta_s$ = 1.9 +/- 0.2 Pas

This means that the error in the specific viscosity is from 10 to 100% ! A reasonable estimate of the error in $[\eta]$ should thus be 60%. Even at the upper limit of this error, $[\eta]$ is still less than the values reported by Yanaki and Noik and Lecourtier. This indicates that the solvent used increased the flexibility of the molecule.

The calculation of L is performed with eq. 3.9. Since L appears in the power 3 the error involved is of 20%. The obtained value of 0.53µm is lower by a factor of 2-3 than the one reported by the above-mentioned authors.

The calculated values of n_1 and n_2 give a rough estimate of the limits in the concentration regimes. From the obtained values it must be concluded that though all

solutions lie in the semi-dilute range, the 100 and 500 ppm solutions should have a behaviour close to that of dilute ones.

Finally, although the different quantities appearing in eq. 3.10 and 3.11 involve important error brackets, the fact that the onset of shear-thinning occurs at $\lambda\dot{\gamma}$ close to 1 indicates that the obtained values of λ are close to the actual ones. It must be stressed here that at $\lambda\dot{\gamma}\cong 1$ the flow is strong enough to orientate the molecules.

3.3.4. The temperature dependence.

Glucose is well-known for the high dependence of its viscosity on the temperature. The viscosity of the 100 ppm solution was measured at four different temperatures (17, 20, 23 and 26 °C). The constant values found at each temperature (Fig. 3.6) are shown in the following table:

Table 3.3 : Viscosity of the 100 ppm solution at different temperatures.

T (°C)	η (Pas)
17	1.80
20	1.27
23	1.03
26	0.81

These data match quite well the Arrhenius relationship:

$$\eta = A\, e^{(B/T)} \qquad (3.12)$$

with $A = 9.05 \cdot 10^{-12}$, $B = 7535.2$ if T is expressed in °K and η in Pas (Fig. 3.7). This corresponds to a very important variation (about 8%/°C) at the temperatures examined.

3.4. The orifice flow.

Orifice flow experiments were performed in the submerged jet configuration with the scleroglucane solutions. The temperature during each orifice experiment is shown in Table 3.4. All temperatures have been included between 20.3 and 21.5°C.

Table 3.4 : The mean temperature during each orifice experiment.

c (ppm)	orifice d (mm)	T (°C)
100	1.2	21.0
500	1.2	20.3
500	0.53	21.5
2000	1.2	20.8
5000	1.2	20.6

Two orifices of respective diameters 1.2 mm and 0.53 mm were used. The flow rate covered the range 10^{-3} ml/s < q_v < 1 ml/s. The flow was visualized. A conical channel was formed by the main flow region as in any earlier experimental study of semi-rigid polymer solutions. A general observation is that the flow curves had much smoother slopes than in the case of the flexible polymer solutions (Fig. 3.8). No derivation from the slope 1 can be detected within the precision of the measurements except for the 100ppm where a low and a high linear regimes are interconnected by a transition zone.

Cartalos and Piau [24] have performed orifice flow experiments with dilute solutions of a partially hydrolyzed polyacrylamide. Repulsive electrostatic charges along the chain backbone result to a semi-rigid rod conformation, which gives flow curves with smooth slopes. They have shown that by adding NaCl, which screens electrostatic charges along the chain backbone, the polymer behaves as a flexible one, giving a behavior similar to the one found in chapter 2. For the unsalted solutions much lower slopes were observed.

Consequently, steep slopes in the flow curves (equal or higher than 2) are indicative of important molecular unravelling. When molecular dimensions do not vary considerably, either due to swelling by electrostatic repulsions as was the case for the unsalted HPAM solutions or due to chain stifness, as is the case in the present results with scleroglucan, the variation of pressure with flow rate is much more progressive.

3.4.1 Analysis of the flow curves

The flow curves were represented in a dimensionless way by the use of the coefficient C' :

$$C' = \frac{P_g}{P_N} = \frac{P_g}{\frac{3}{4}\pi\eta\dot{\gamma}} \qquad (3.13)$$

which denotes the ratio of the pressure loss to that necessary to push through the orifice a Newtonian fluid of the same viscosity. This definition of the dimensionless pressure drop is more appropriate for constant viscosity fluids. In the case of suspensions of slender rigid particles, particle alignment with flow should be considered for the calculation of η in eq. 3.13. In fact, as shown by a series of papers by Hinch and Leal [10-12], when particles are aligned, the viscosity of the suspension is greater than the solvent viscosity by a factor approximately equal to (1/r), where r is the aspect ratio. In our case, molecules are submitted to an elongational field that is very efficient in orienting particles. Since r is of the order of 100, we take $\eta = \eta_s$ in (3.13). For this reason, the viscosity of the solvent has been used in the calculation of the C' coefficient.

Two regimes of constant values of the coefficient C' plotted as a function of the shear rate can be distinguished (Fig. 3.9), for the 100 ppm solution :

- An initial Newtonian regime at low flow rates where C' is close to 1 and the flow field is like the one for a newtonian fluid, and
- A higher regime where C' is constant indicating a constant elongational viscosity from the Binding analysis (annex C) and the flow field is characterised by an elastic convex vortex.

An intermediate regime exists between these two regimes where C' is increasing.

During the first Newtonian regime the stiff-chain polymer molecules are uniformly oriented. During the intermediate transition regime molecules start to be oriented by the flow. The final higher regime finds the molecules fully aligned.

Our observations extend in all three regimes as far as the 100ppm solution is concerned. Departure from the Newtonian regime occurs at $\lambda\dot{\gamma} = 3.5$. The final regime is reached for $\lambda\dot{\gamma} = 10$. For the more concentrated solutions, where orifice measurements at $\lambda\dot{\gamma} > 10$ are available, the final regime of constant C' is only observed. The upper value of the C' coefficient is about 1.35 for the 100ppm solution and 2.15 for the 500ppm solution (d=1.2mm). The difference observed with the smaller diameter (d=0.53mm) for the 500ppm solution should be due to the fact that there has been a difference in the temperature of the two experiments of 0.8°C. Moreover, the measurements in high regimes with the d=0.53mm orifice have been strongly influenced by inertia as will be shown in the following. The C' coefficient was about 6 for the 5000ppm solution and about 4 for the 2000ppm solution.

Pictures of the flow for the 2000ppm solution are shown in Fig. 3.10. This series shows departure from a near Newtonian flow structure and growth of the viscoelastic corner vortex.

The evolution of the re-attachment length of the vortices X (which will be also discussed later on), is examined in Fig. 3.12. This flow parameter is plotted as a function of the product $(\lambda\,\dot{\gamma})$.

For the 100 ppm solution, X reaches a constant value X_∞ at $\lambda\dot{\gamma} = 3.5$, which is very close to the onset of the transition regime. As concentration is increased, the value of $(\lambda\,\dot{\gamma})$ where X_∞ is reached, is increased. On the flow of the 500 ppm solution through the 0.53 mm orifice, X is decreasing under the influence of inertia as will be shown further on. The sudden increase of the vortex height seems to be triggered in the same $\lambda\dot{\gamma}$ value for the two lowest concentration solutions. For the two highest concentration solutions , the vortex growth starts at higher $\lambda\dot{\gamma}$ values. At the highest regimes examined, the vortex heights of the 2000 and 5000ppm solutions tend to join each other.

3.4.2. Instabilities observed.

Instabilities have been observed during the flow of all scleroglucane solutions except for the 100ppm one. With the increase of the flow rate, back and forth oscillations along the particle pathline in the main flow region appeared. This phenomenon has already been observed in the previous chapter with flexible solutions. At higher regimes, the lateral oscillations mentioned as S-form instability in Chapter 2 occurred here too. These oscillations persisted up to the highest regimes examined. We nevertheless have to mention here that the amplitude of all these oscillations has been much smaller than in the case of the PEO solutions of the previous chapter.

The value of the flow parameters during the onset of the instabilities is given in the table that follows for every solution :

Table 3.5 : Values of the flow parameters for the onset of the instabilities.

solution	d (mm)	solvent glucose/wat.	qv $(10^{-3}ml/s)$	Pg (mbar)	$\dot{\gamma}$ (s^{-1})
500ppm	0.53	80/20	73.0	300.0	4994
500ppm	1.2	80/20	30.0	11.4	177
2000ppm	1.2	90/10	59.6	165.7	351
5000ppm	1.2	80/20	17.6	18.4	103

In the previous chapter, for flexible polymer solutions, the critical parameter for the knitting instability was found to be the ratio of the elongational stress to the shear stress at the wall in the level of the orifice : S_{el}. We have shown there that the onset of three-dimensional instabilities was connected to a value of about 12 of this parameter.

According to the Binding analysis (Annex C), the stretch rate on the axis at the orifice level varies with :

$$\dot{\varepsilon} \approx \dot{\gamma}^{(1+n)/(1+t)} \qquad (3.14)$$

where n and t are the coefficients of the power-law expressions for the elongational and shear viscosities :

$$\eta_S = k\,\dot{\gamma}^{n-1} \qquad (3.15) \qquad\qquad \eta_E = l\,\dot{\varepsilon}^{t-1} \qquad (3.16)$$

In the present case, since the fluids considered have an almost constant viscosity, it is n = 1 and , as it can be easily shown t = 1. The stretch rate varies thus with $\dot{\gamma}$ and the ratio S_{el} is independent of the regime. For the presently examined flow of the scleroglucane solutions it takes values varying from 3.2 to 5. This is much lower than the values of around 12, found for flexible polymers to characterize the onset of 3D unstable flow. It can be concluded that 3D unstable flow is not observed in the present case because the elongationnal stress levels remain low.

3.4.3. The vortex re-attachment length.

By visualizing the flow and taking pictures of it (Annex B), measurements of the vortex reattachment length:

$$X = \frac{L_v}{D_u} \qquad (3.17)$$

(where L_v is the length of the vortex and D_u the upstream tube diameter), were carried out. Binnington and Boger [4] have previously compared vortex length data of semi-rigid solutions (both macro: glass fibers and micro: xanthan gum) with flexible ones (polyacrylamide). While PAA gave enormous vortex growth in a very small region of shear rates (Fig. 3.11), semi-rigid rods gave almost constant vortex length. As shown in Fig. 3.11, scleroglucane solutions give considerable vortex growth.

The re-attachment length of the 100 ppm fluid passes from 0.17 (the value for Newtonian flow) to 0.29 and it stabilizes at this value. The 500 ppm fluid develops

larger vortices and X stabilizes at 0.56 for $\dot{\gamma} > 40\ s^{-1}$. The X of the 5000 ppm fluid covers the whole range from 0.2 to 0.7. The essential difference between flexible and semi-rigid solutions is, thus, the rate of increase of the vortices: With the former ones there is a rapid transition from a Newtonian cell size through to larger dimensions and ultimately to unstable rotational and pulsing cell movement. With the latter, vortex growth occurs in a more gradual way. By comparing for example the PAA solution in [4] (Fig. 3.12), X passes from Newtonian cell size to 0.55 from $\dot{\gamma}_1 = 7\ s^{-1}$ to $\dot{\gamma}_2 = 30\ s^{-1}$ while for the 5000 ppm scleroglucane the same growth is obtained from $\dot{\gamma}_1 = 4\ s^{-1}$ to $\dot{\gamma}_2 = 200\ s^{-1}$.

We measured the angle α which is formed by the vortex and the direction of the flow in the entry region. This angle shows a monotonic decrease and attains a high regime asymptotic value α_∞ (Fig. 3.15). The value of α_∞ is plotted as a function of concentration (Fig. 3.16).

The evolution of X and α with $\lambda\dot{\gamma}$ is plotted on Fig. 3.12. Various observations arise from this graph :

When solutions are close to the dilute range (100 - 500ppm), departure from the newtonian field structure occurs at $\lambda\dot{\gamma} \cong 1$. The subsequent increase of the viscoelastic vortex seems to be independent of concentration, but the $\lambda\dot{\gamma}$ where X reaches the asymptotic value X_∞ and X_∞ increase with concentration. Also X and α reach their asymptotic values at approximately the same $\lambda\dot{\gamma}$ for each concentration.

For semi-dilute solutions (2000 and 5000ppm), the whole evolution of X and α with $\lambda\dot{\gamma}$ depends on concentration. The value of $\lambda\dot{\gamma}$ characterising the onset of viscoelastic effects increases with c. It seems that during the vortex growth regime, the scaling of X with $\lambda\dot{\gamma}$ is the same as the one with dilute solutions. The initial relatively steep increase of X is followed by a smoother increase. The $\lambda\dot{\gamma}$ value where the change of slope occurs corresponds to the value where α reaches an asymptotic value.

Constant X and α values indicate that the fluid material properties attain constant values in the whole part of the converging zone upstream of the orifice. In a suspension of fibers this should occur when fibers are completely aligned with the flow lines. Our results indicate that, for dilute solutions, complete alignment is achieved for $\lambda\dot{\gamma}$ from 3 to 50. For semi-dilute solutions, as concentration is increased, neighbouring fibers hinder alignment, so higher $\lambda\dot{\gamma}$ values are needed.

3.4.3.1. Stabilization at high regimes.

As the regime increases, the vortex growth is followed by a region where the vortex height remains insensible to the flow rate. The dependence of X_∞ (the limiting value of X) on concentration is compared in Fig. 3.13 with other theoretical and

experimental studies. Good agreement is found with the former studies. The slope of the increase of X_∞ with ϕ is similar and even the absolute values of X_∞ are close. Our results show that a limiting value of the parameter X_∞ should exist with concentration.

The results of Lipscomb et al should be compared to ours from the point of view of nL^3 (concentration regime) and $\lambda\dot{\gamma}$ (intensity of the flow field. Although the range of nL^3 covered in Lipscomb et al is comparable to ours (6.75 to 106 as compared to 2.44 to 122 in this study), much higher $\lambda\dot{\gamma}$ were explored in their study : since L is 3mm, that is 5000 times greater than the scleroglucan molecule, λ values are expected to be several orders of magnitude higher than ours (see eq. 3.9 and 3.10). This means that the $\lambda\dot{\gamma}$ values in Lipscomb et al correspond to much higher regimes than those studied in the present work, which can explain why constant X values are observed for all flow rates in their work.

3.4.3.2. The role of inertia.

As previously indicated, inertia crushes the vortices once it becomes important. Boger et al [15] compare experimental observations of the influence of the Reynolds number on X with predictions of Kim-E et al [16], which match very well. According to these predictions it is slightly above Re= 0.1 that vortices start to shrink, and above Re= 1 this shrinkage becomes considerable. Chiba et al predict a considerable decrease of X for Re > 1. Our orifice experiments included in general low Reynolds numbers (Re <1), with the exception of the 500 ppm through the 0.53 mm orifice. In this experiment (Fig. 3.14) vortices start to diminish indeed at Re= 0.3 and continue till Re= 3 where observations exist.

3.4.3.3. The role of the contraction ratio.

By comparing the two different orifice diameter experiments with the 500 ppm solution, we notice that X does not change with the contraction ratio β (Fig. 3.11). Lipscomb et al predict a slight increase of X with β in the range $3 < \beta < 6.5$. Our results indicate that at high contraction ratios (16.7 and 37.7), X becomes independent of contraction ratio.

3.5. The extensional viscosity.

The orifice flow data were used to calculate the extensional viscosity of the scleroglucane solutions by the method of Binding (Appendix C). According to this analysis, for a constant viscosity fluid and when the slope of the pressure drop-flow rate relation is linear, the extensional viscosity is constant, that is $l=\eta_E$. Furthermore :

$$P_g = \frac{2}{3} D \eta_s \dot{\gamma} \qquad (3.18)$$

where :

$$D = \left(\frac{8}{3}\frac{\eta_E}{\eta_s}\right)^{1/2} \qquad (3.19)$$

In (3.18) and (3.19) we replaced the shear viscosity value η by η_s, following the arguments developed in section 3.4.1.
By combining (3.18) and (3.19), we obtain :

$$\frac{\eta_E}{3\eta_s} = \frac{9}{32}\left(\frac{P_g}{\eta_s \dot{\gamma}}\right)^2 \qquad (3.20)$$

The left member of (3.20) is the Trouron ratio.

On the other hand, the analysis of Batchelor for non-dilute suspensions predicts the elongational viscosity as a function of the shear viscosity of the solvent η_s, the length of the expanded chain L, its equivalent diameter b and the volume concentration $\phi = nv$, where $v = \frac{\pi b^2}{4} L$ the volume of a single particle :

$$\frac{\eta_E}{3\eta_s} = \frac{\pi L^3 n}{9 \operatorname{Log}\left(\frac{\pi}{\phi}\right)} + 1 \qquad (3.21)$$

This analysis is valid if the solution concentration is such that :

$$b << H << L \qquad (3.22)$$

where H is the average distance between the rods in the plane normal to the chain axes. This distance is given by :

$$H = (nL)^{-\left(\frac{1}{2}\right)} \qquad (3.23)$$

where n is the number of rods per unit volume.

The different quantities involved in eq. (3.20) and (3.21) are shown in tables 3.6 and 3.7. If the value of L=0.53μm derived under static conditions (intrinsic viscosity at zero shear rate) is used, then the Batchelor analysis gives much lower results for the Trouton ratio than the Binding analysis. Since molecular flexibility is increased by the solvent used, molecular extension should be taken into account. Thus the value of L=1.2μm corresponding to an extension of about 2.2 was also used (last column in table 3.7). With this value, the agreement between the Batchelor and the Binding analyses is considerably improved. Note that L=1.2μm is comparable to the values reported by Yanaki and Noik and Lecourtier for the scleroglucan molecule. The values of the Trouton ratio obtained with L=1.2μm for the Batchelor analysis differ by less than 20% from those obtained by the Binding analysis for c≥500ppm. For the 100ppm solution the greater discrepancy observed is attributed to the fact that H is comparable to L, which disagrees with the assumptions of the Batchelor analysis.

Table 3.6 : Elongational viscosity from the Binding analysis.

solution	$P_g / \dot{\gamma}$ (Pas)	$P_g / \eta_s \dot{\gamma}$	H (μm)	$\eta_E / 3\eta_s$ (Binding)
100ppm	4	3.33	0.33	3.13
500ppm	6.25	5.21	0.15	7.63
2000ppm	45.0	8.82	0.076	21.8
5000ppm	17.5	14.6	0.048	59.8

Table 3.7 : Elongational viscosity from the Batchelor analysis.

solution	$n\,(\mu m^{-3})$	ϕ	H (μm)	$\eta_E / 3\eta_s$ (L=0.53μm)	$\eta_E / 3\eta_s$ (L= 1.2μm)
100ppm	16.4	$6.14\ 10^{-5}$	0.33	1.08	1.91
500ppm	82.0	$3.07\ 10^{-4}$	0.15	1.51	6.86
2000ppm	328	$1.23\ 10^{-3}$	0.076	3.17	26.2
5000ppm	820	$3.07\ 10^{-3}$	0.048	7.14	72.3

Direct comparison of our extensional viscosity results with other experimental results is difficult, since little data on similar fluids exists in the literature. Khagram et

al [17] have performed fiber-spinning measurements on aqueous xanthan gum solutions of low concentrations (300 to 500 ppm). The molecular weight of their polymer is much higher than our scleroglucane ($12 \cdot 10^6$). They find Trouton ratios, independent of the stretch rate, of about 105. Fuller et al [18] used the opposing jets technique on xanthan gum solutions (Mw about 10^7) of very low concentration (50 to 100 ppm), in glycerin/water mixtures. They find again essentially higher values than ours (varying from 30 to 150 depending on the concentration).

A further point in the analysis of Binding can be examined through the values obtained for α. According to this analysis,

$$\left(-\frac{dR}{dz}\right) = \left(2\frac{\eta_{E\infty}}{3\eta_s}\right)^{-\frac{1}{2}} \qquad (3.24)$$

when $\eta_{E\infty}$ and η_s are constant ($t = n = 1, l = \eta_{E\infty}, k = \eta_s$). But

$$\left(-\frac{dR}{dz}\right) = tg\alpha \qquad (3.25)$$

The evolution of $tg\alpha$ with $\frac{\eta_{E\infty}}{3\eta_s}$ (table 3.6) is shown in Fig. 3.17. The scaling law is close to (-1/2), the theoretical prediction, which shows coherence of our results with the analysis of Binding. However, the experimental velue in the relationship between $tg\alpha$ and $\left(\frac{\eta_{E\infty}}{3\eta_s}\right)^{-\frac{1}{2}}$ is greater than the theoretical value of $\left(\frac{1}{\sqrt{2}}\right)$ by about 40%.

3.6. Conclusion.

Experiments on scleroglucane (semi-rigid) solutions are presented in this chapter. In order to avoid inertia during orifice flow, a glucose-syrup was also used as a solvent. The shear viscosity of these solutions was first measured. The solutions were found to cover the transition between the dilute and the semi-dilute regime and extend to the semi-dilute regime.

Orifice flow experiments have been performed with these solutions. Scalings of the flow curves and evolution of the flow structure is shown to depend on flow regime and concentration. At low flow regimes where flow strength cannot orient the molecules, solution behaviour is newtonian. Departure from Newtonian behaviour is characterised by a typical Peclet number, the product of the time λ characterising rotational diffusion and the average deformation rate $\dot{\gamma}$. λ is calculated from the Doi-Edwards theory and is shown to characterise the onset of shear-thinning in shear flow.

For dilute solutions, the onset of viscoelastic effects takes place at $\lambda\dot{\gamma} \cong 3$. For $\lambda\dot{\gamma}$ between 3 to about 10, flow is characterised by a transition regime where the main feature is the evolution of molecular alignment along the streamlines. As a result, the relation between pressure drop and flow rate is linear and the vortex reattachment length and the slope of the vortex boundary on the orifice plane become independent of flow rate.

For solutions in the semi-dilute range, the results indicate that neighbouring molecules hinder alignment, so higher $\lambda\dot{\gamma}$ values are required for molecular orientation. Due to the very high values of λ, only the end of the transition regime and the beginning of the final linear regime were within the range of experimental observations. Results in the literature also cover the final regime, where the vortex length is independent of the flow rate.

Our results for dilute solutions show that, as expected, the vortex re-attachment length varies from the newtonian value at very low flow rates (the higher the length and so the λ value, the lower the $\dot{\gamma}$ where Newtonian behaviour occurs) where molecules are randomly oriented, to a constant value at high flow regimes where molecules are fully aligned. For semi-rigid molecules where molecular orientation is the basic phenomenon, vortex growth is much slower than in solutions of flexible molecules, where in addition important molecular deformation takes place.

The transition regime that separates the newtonian from the asymptotic high flow rate regime, remains to be studied for the semi-dilute solutions. As shown, the basic problem is that, due to important aspect ratios of the semi-rigid macromolecules very high relaxation times characterise the solution. Observation should be performed at extremely low flow regimes. Further experiments are needed in order to establish how the pressure drop scales with the flow rate and how X and α vary with $\lambda\dot{\gamma}$ in this regime.

The extensional properties were determined by the Binding analysis. This analysis shows that when P_g is linear with q_v for a constant viscosity fluid, the extensional viscosity is constant. Another prediction of the Binding analysis was verified : the variation of the limiting value of the slope of the vortex boundary as the Trouton ratio to the power (-1/2). The analysis of Batchelor predicts also a constant Trouton ratio when molecules are fully aligned with the streamlines. Good agreement is shown to exist between the two theories, provided molecular extension - although much smaller than the one expected for flexible molecules - is considered.

References

1. H.A. Barnes, J.F. Hutton and K. Walters, "An Introduction to Rheology", Elsevier, 1989.
2. J. Mewis and A.B. Metzner, "The rheological properties of fibres in Newtonian fluids subjected to extensional deformations", J. of Fluid Mechanics, 62 (1974) 593-600.
3. G. K. Batchelor, "The stress generated in a non-dilute suspension of elongated particles by pure straining motion", J. of Fluid Mechanics, 46 (1971) 813-829.
4. R.J. Binnington and D.V. Boger, "Entry flow of semi-rigid rod solutions", J. Non Newt. Fluid Mech., 26 (1987) 115-123.
5. G.G. Lipscomb, M.M. Denn, D.U. Hur and D.V. Boger, "The flow of fiber suspensions in complex geometries", J. Non Newt. Fluid Mech., 26 (1988) 297-325.
6. K. Chiba, K. Nakamura and D.V. Boger, "A numerical solution for the flow of dilute fiber suspensions through an axisymmetric contraction", J. Non Newt. Fluid Mech., 35 (1990) 1-14.
7. R. A. Keiller, M. Rallison and J. G. Evans, "Sink flows of a suspension of rigid rods : the failure of a similarity solution", J. Non Newt. Fluid Mech., 42 (1992) 249-266.
8. R. A. Keiller and E. J. Hinch, "Corner flow of a suspension of rigid rods", J. Non Newt. Fluid Mech., 40 (1991) 323-335.
9. S. M. Dinh and R. C. Armstrong, J. of Rheology, 28 (1984) 207.
10. E. J. Hinch and L. G. Leal, "The effect of Brownian motion on the rheological properties of a suspension of non-spherical particles", J. of Fluid Mech., 52 (1972) 683.
11. E. J. Hinch and L. G. Leal, "Time-dependent shear flows of a suspension of particles with weak Brownian rotations", J. of Fluid Mech., 57 (1973) 753.
12. L. G. Leal and E. J. Hinch, "", Rheologica Acta, 12 (1973) 127.
13. B. E. Vugmeister, C. Wang and H.D. Ou-Yang, "Orientational ordering of rigid rod polymers in shear flow", Mat. Res. Soc. Symp. Proc., Vol. 289, (1993) 63-68.
14. G. H. McKinley, W. P. Raiford, R. A. Brown and R. C. Armstrong, "Nonlinear dynamics of viscoelastic flow in axisymmetric abrupt contractions", J. of Fluid Mechanics, 223 (1991) 411-456.
15. D. V. Boger, D. U. Hur and R. J. Binnington, "Further observations of elastic effects in tubular entry flows", J. Non Newt. Fluid Mech., 20 (1986) 31-49.

16. M.E. Kim, R. A. Brown and R.C. Armstrong, "The roles of inertia and shear-thinning in flow of an inelastic fluid through an axisymmetric sudden contraction", J. Non Newt. Fluid Mech., 13 (1983) 341-363.
17. M. Khagram, R. K. Gupta and T. Sridhar, "Extensional flow of xanthan gum solutions", J. of Rheology, 29 (1985) 191-207.
18. G. G. Fuller, C. A. Cathey, B. Hubbard and B. E. Zebrowski, "Extensional viscosity measurements of low viscosity fluids", J. of Rheology, 31 (1987) 235-249.
19. T. Yanaki and T. Norisuye, "Triple helix and random coil of scleroglucane in dilute solution", Polymer J., 15 (1983) 389-396.
20. T. Yanaki, T. Kojima and T. Norisuye, "Triple helix of scleroglucane in dilute aqueous sodium hydroxide", Polymer J., 13 (1981) 1135-1143.
21. R. Nardin and M. Vincendon, "Isotopic exchange study of the scleroglucan chain in solution", Macromolecules, 22 (1989) 3551-3554.
22. T. Itou, A. Teramoto, T. Matsuo and H. Suga, "Ordered structure in aqueous polysaccharide. Cooperative order - disorder transition in aqueous schizophyllan", Macromolecules, 19 (1986) 1234-1240.
23. C. Noik and J. Lecourtier, "Studies of scleroglucane conformation by rheological measurements versus temperature up to 150°C", Polymer, 34 (1993) 150-157.
24. U. Cartalos and J.M. Piau, "Creeping flow regimes of low concentration polymer solutions in thick solvents through an orifice die", J. Non Newt. Fluid Mech., 45 (1992) 231-285.
25. M. Doi and S. F. Edwards, "The theory of polymer dynamics", Oxford Science publications, Clarendon Press, Oxford, 1986.
26. R. G. Larson, "Constitutive equations for polymer melts and solutions", Butterworths Series Ed., 1987.

TABLES AND FIGURES

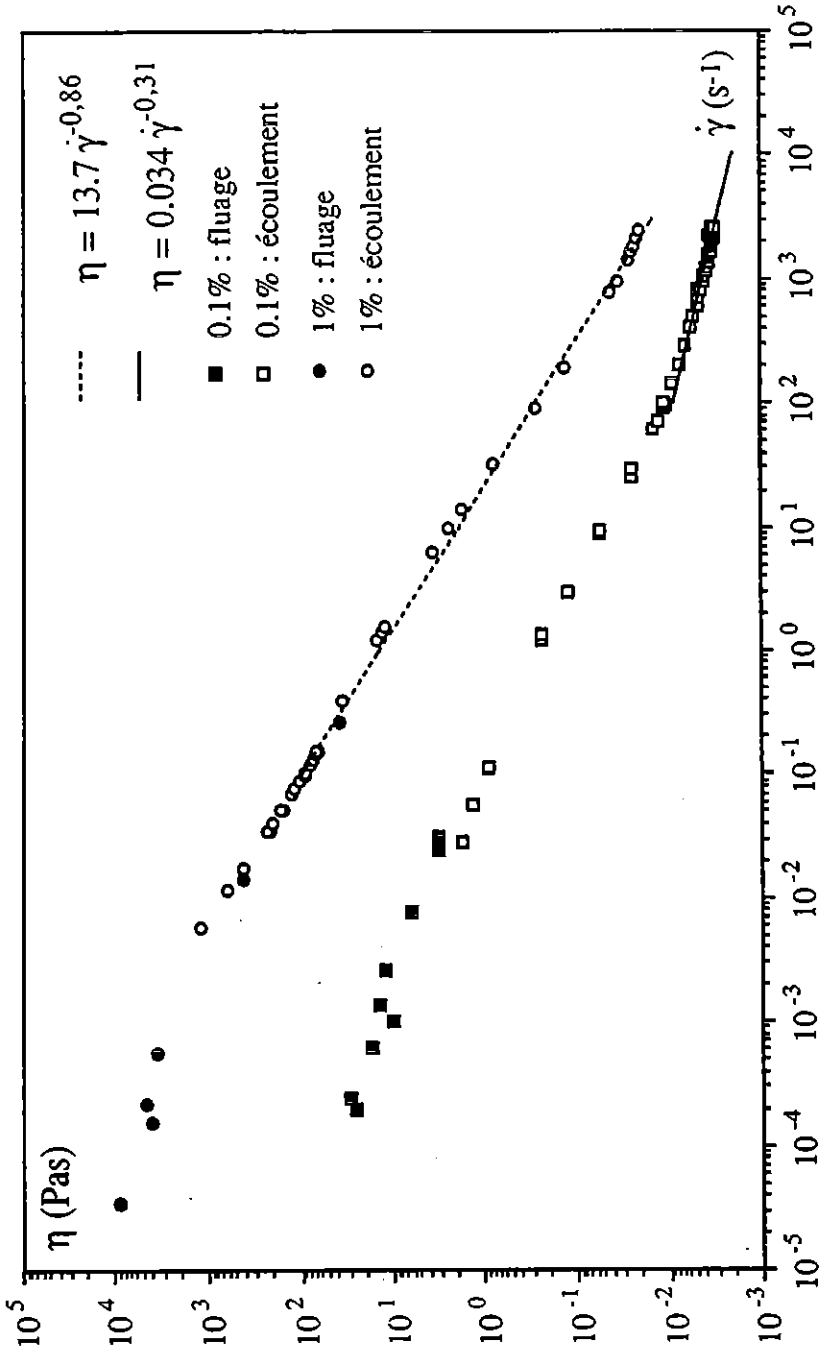

Figure 3.1 : Shear viscosity of the aqueous scleroglucane solutions

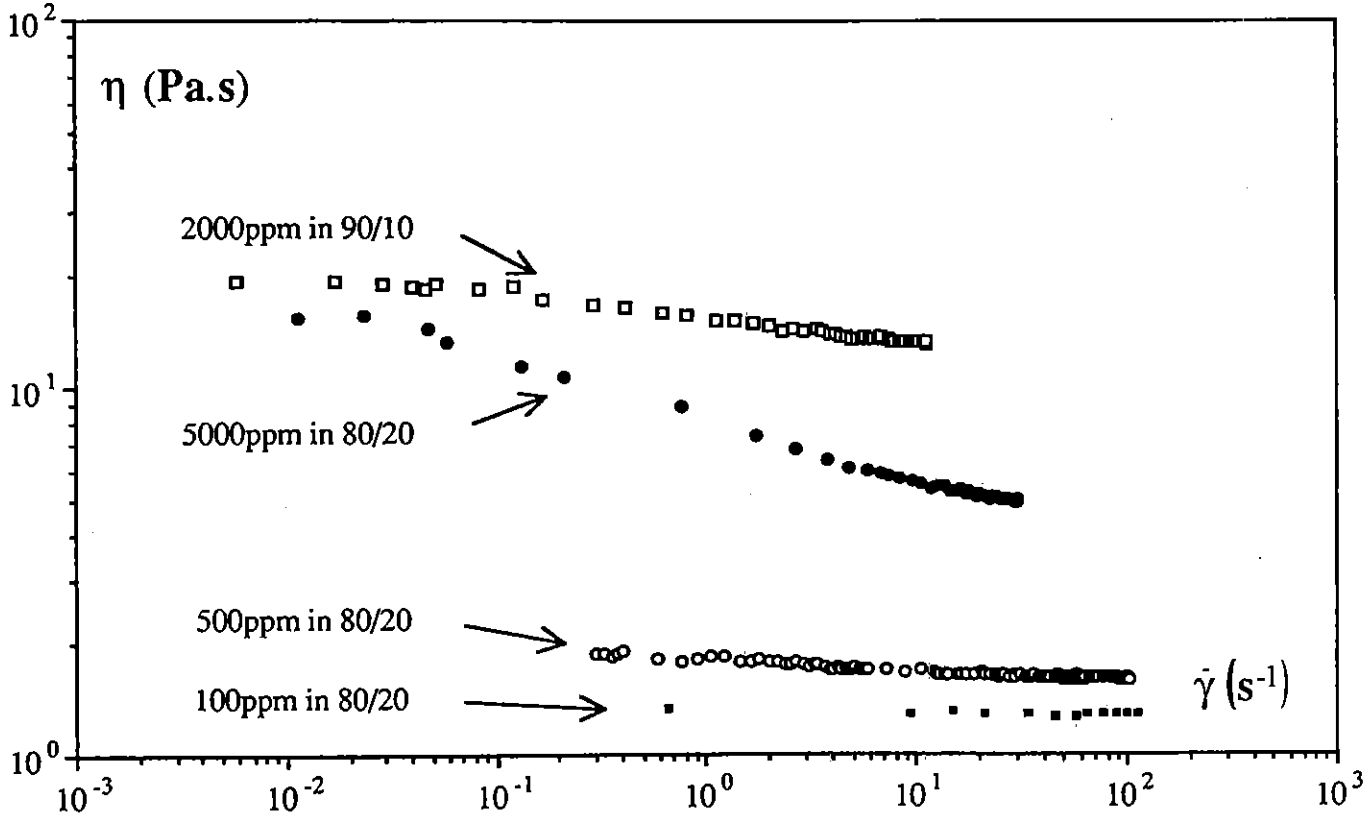

Figure 3.2 : Shear viscosity of the scleroglucane solutions in the glucose syrup at 20°C

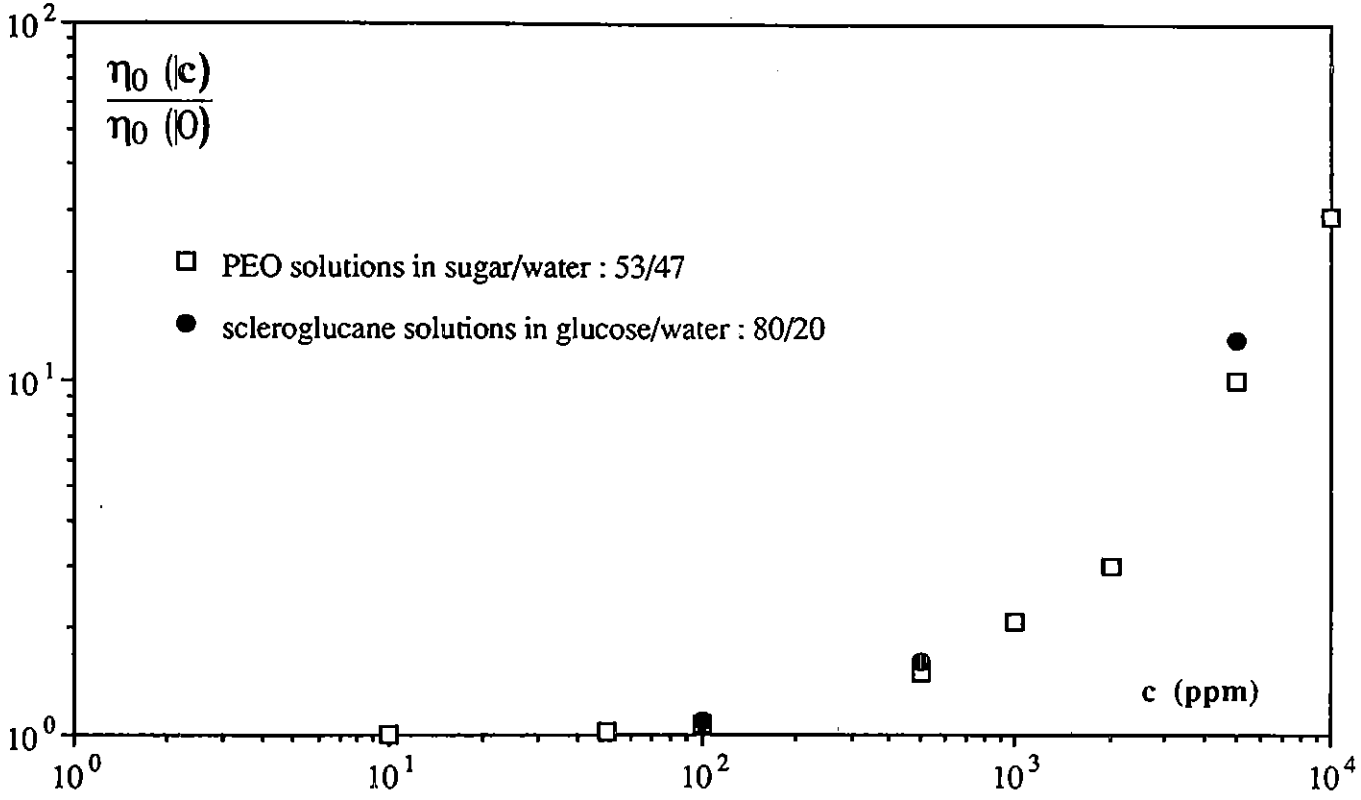

Figure 3.3 : Ratio of the zero shear viscosity to the solvent viscosity for the scleroglucane and PEO solutions

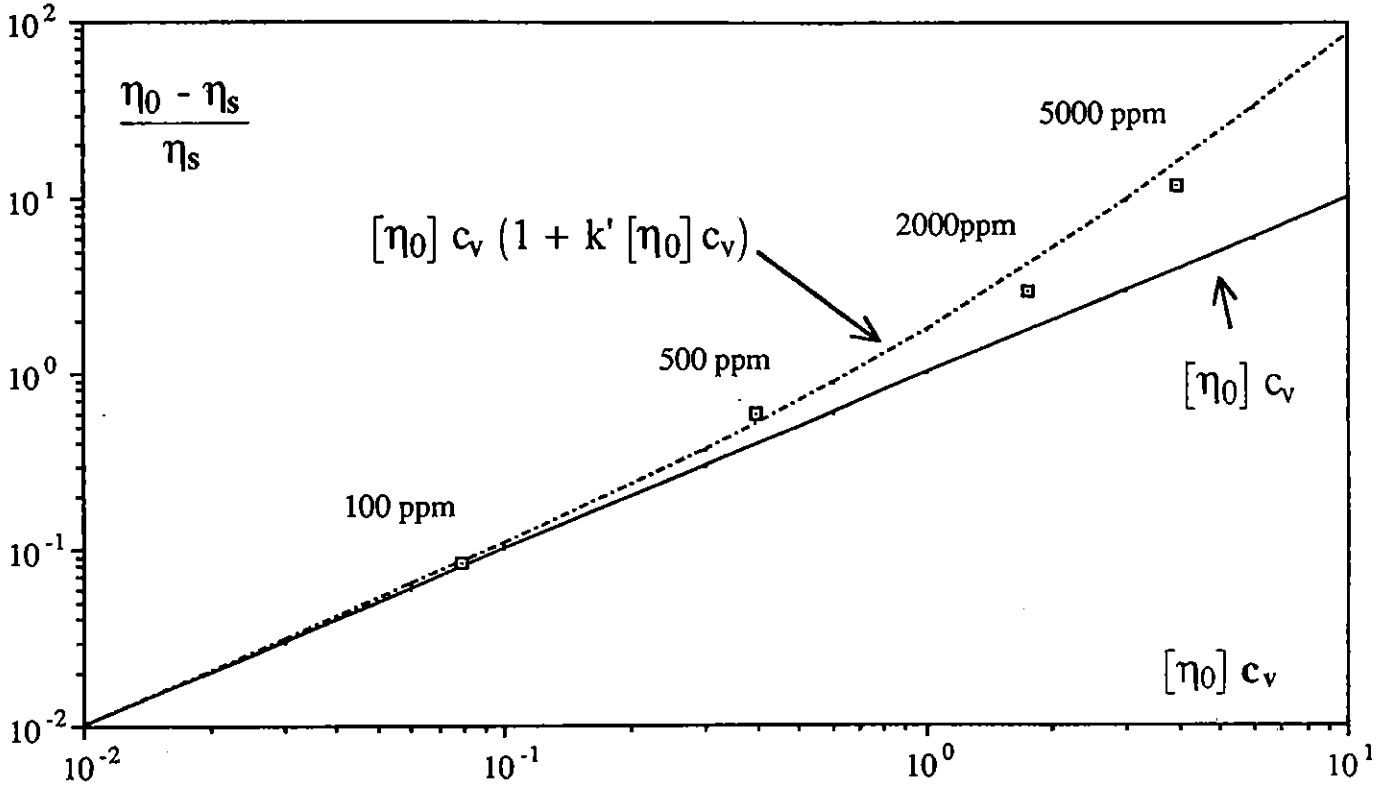

Figure 3.4 : Specific viscosity versus the reduced concentration for the scleroglucane solutions

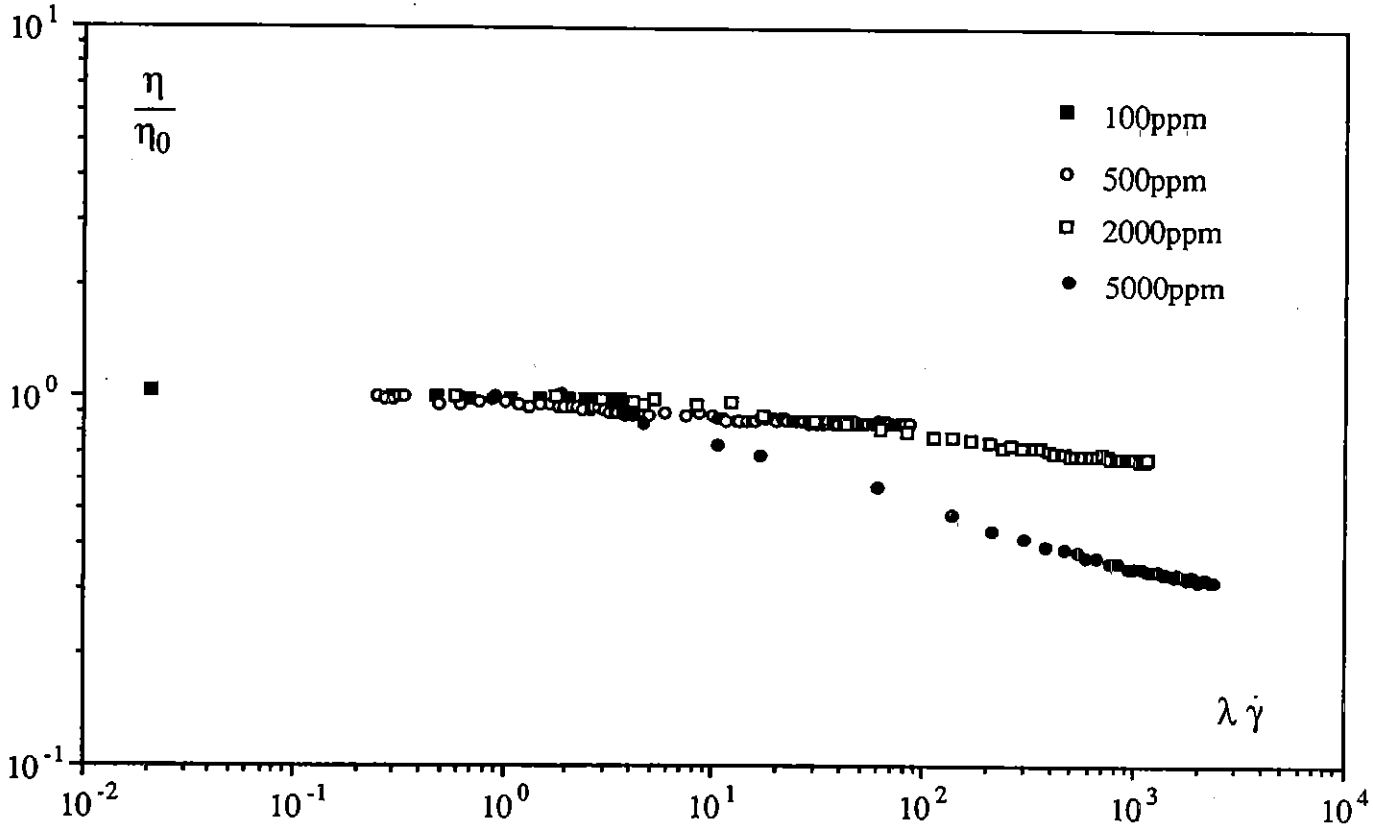

Figure 3.5 : Reduced shear viscosity versus dimensionless shear rate for the scleroglucane solutions

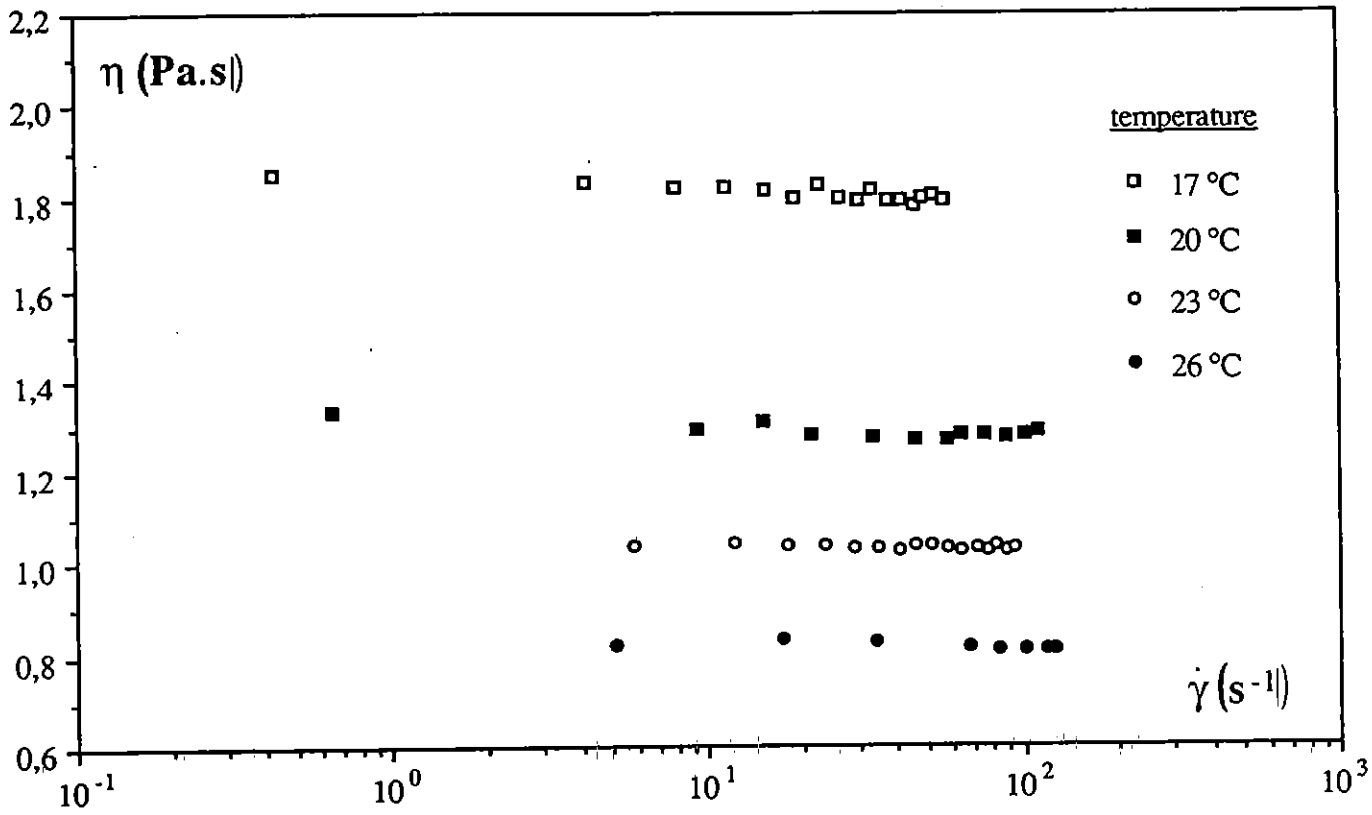

Figure 3.6 : Shear viscosity of the 100 ppm scleroglucane solution for different temperatures

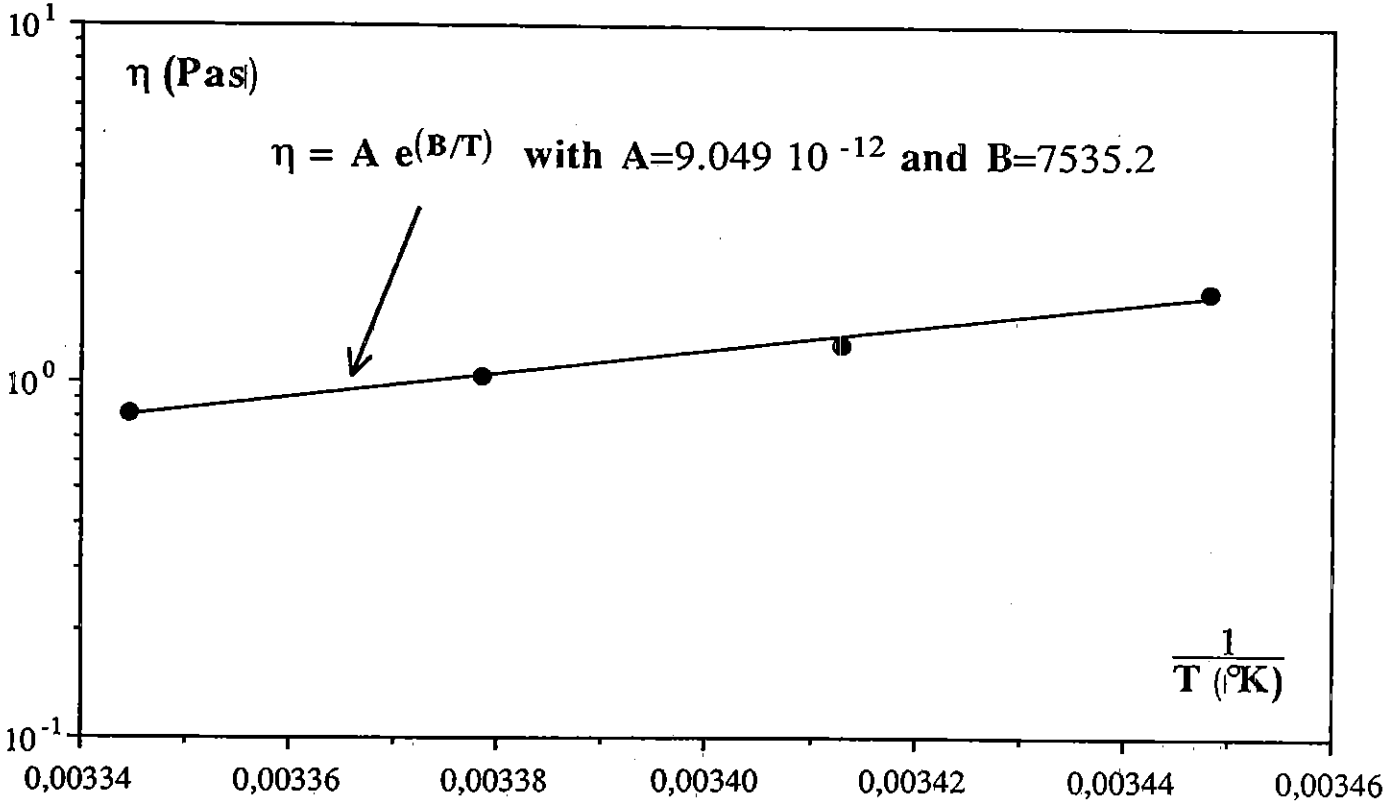

Figure 3.7 : Influence of the temperature on the shear viscosity of the 100 ppm scleroglucane solution

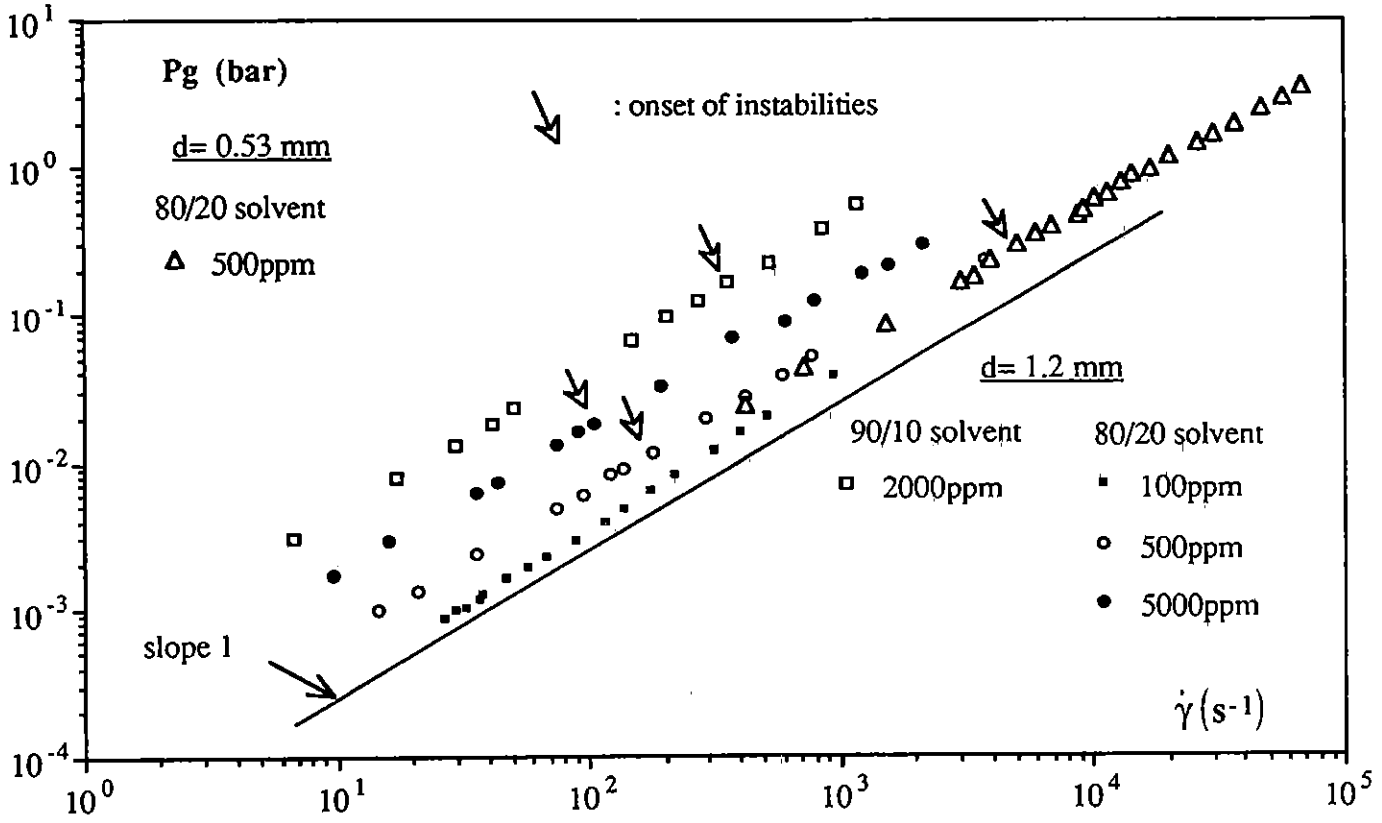

Figure 3.8. Flow curves of the thickened scleroglucane solutions

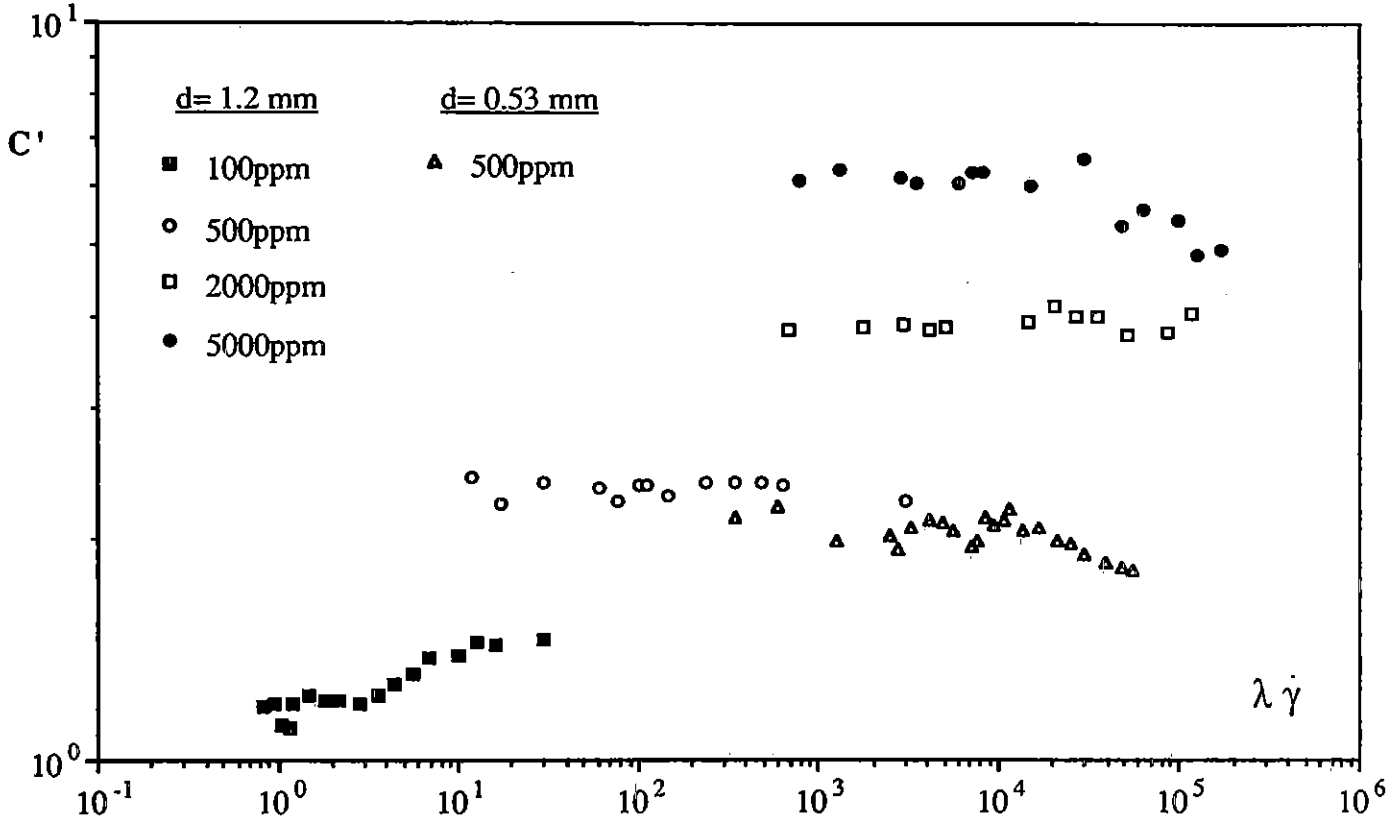

Figure 3.9 : C' number versus reduced shear rate

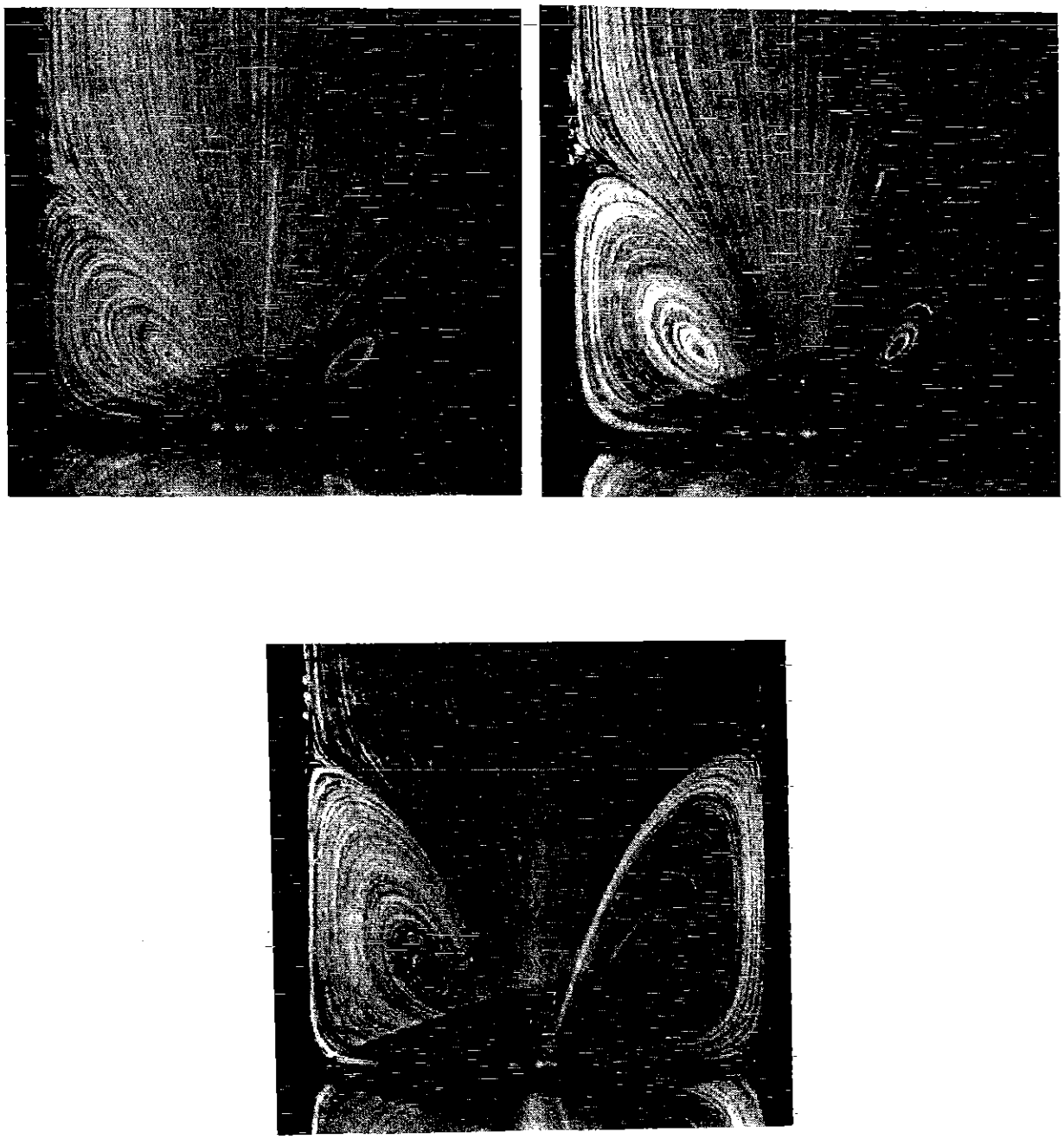

Figure 3.10. Flow visualization of the 2000 ppm scleroglucane solution (Φ= 1.2 mm).
(a) V= 2.6 mm/s, $\dot{\gamma}$= 17.3 s^{-1}, Re= 1.02 10^{-4}, T= 30 min.
(b) V= 21.8 mm/s, $\dot{\gamma}$= 145.4 s-1, Re= 4.01 10^{-3}, T= 10 min.
(d) V= 77.2 mm/s, $\dot{\gamma}$= 514.6 s^{-1}, Re= 1.5 10^{-2}, T= 4 min.

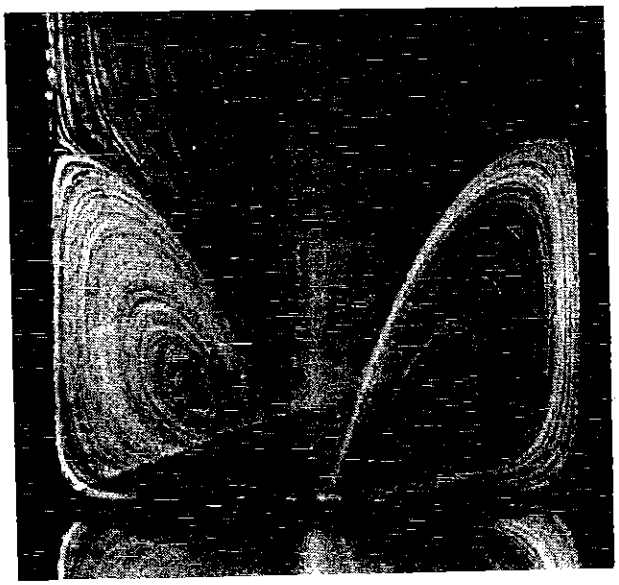

Figure 3.10. Flow visualization of the 2000 ppm scleroglucane solution (Φ= 1.2 mm).

(a) V= 2.6 mm/s, $\dot{\gamma}$= 17.3 s^{-1}, Re= 1.02 10^{-4}, T= 30 min.

(b) V= 21.8 mm/s, $\dot{\gamma}$= 145.4 s-1, Re= 4.01 10^{-3}, T= 10 min.

(d) V= 77.2 mm/s, $\dot{\gamma}$= 514.6 s^{-1}, Re= 1.5 10^{-2}, T= 4 min.

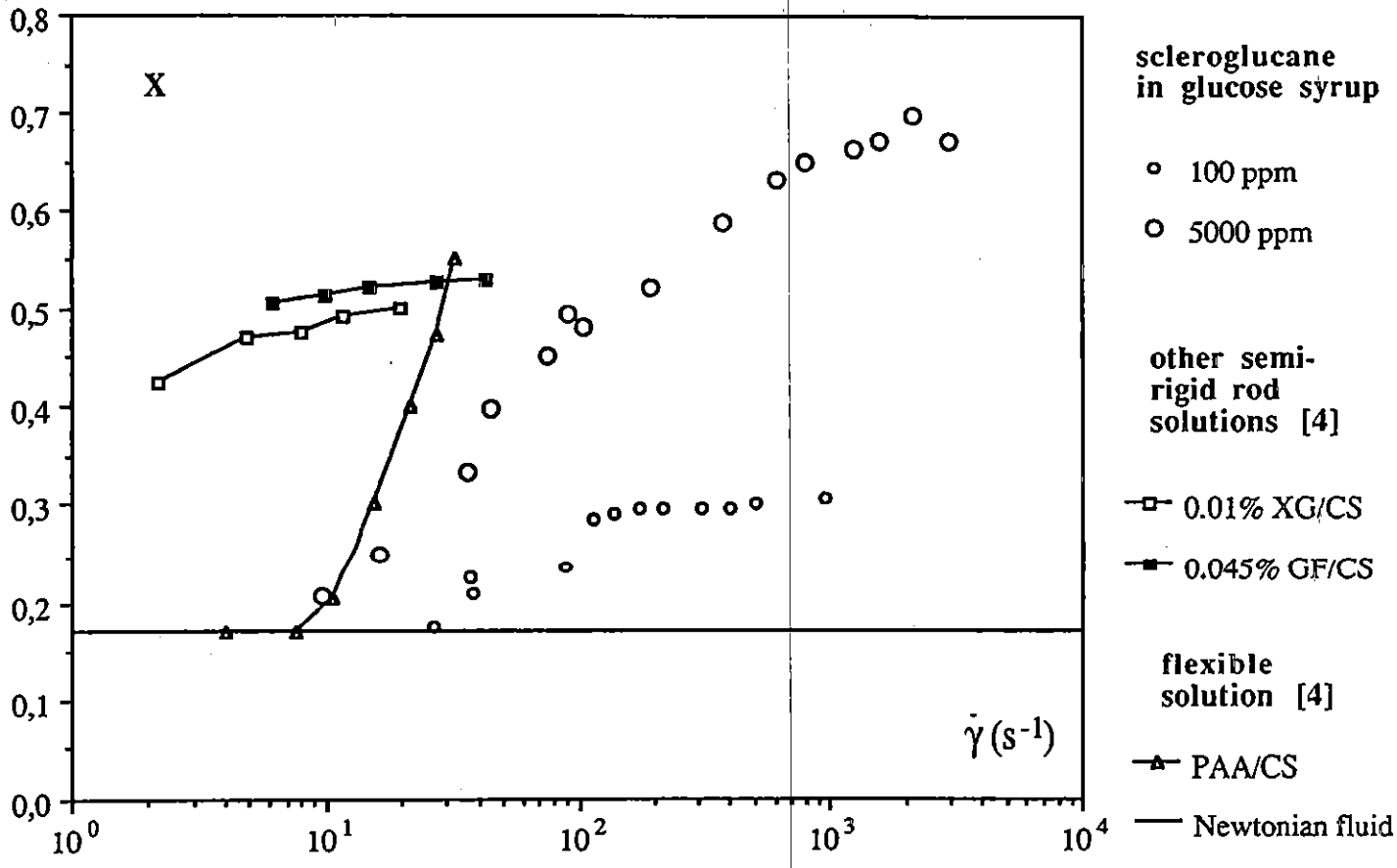

Figure 3.11 : Influence of the regime on the reduced vortex height. Comparison with other studies

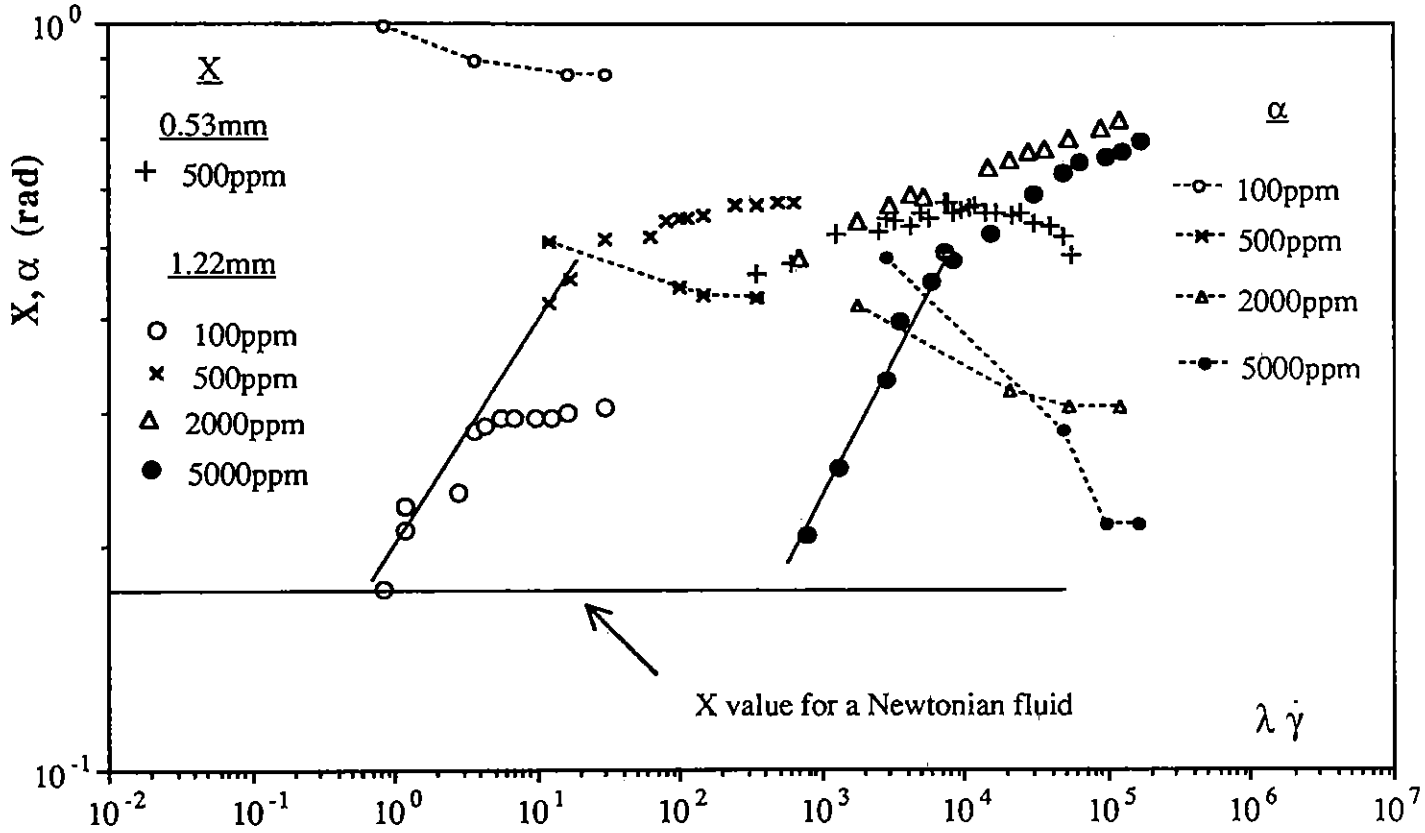

Figure 3.12 : Reduced vortex height and vortex angle versus reduced shear rate

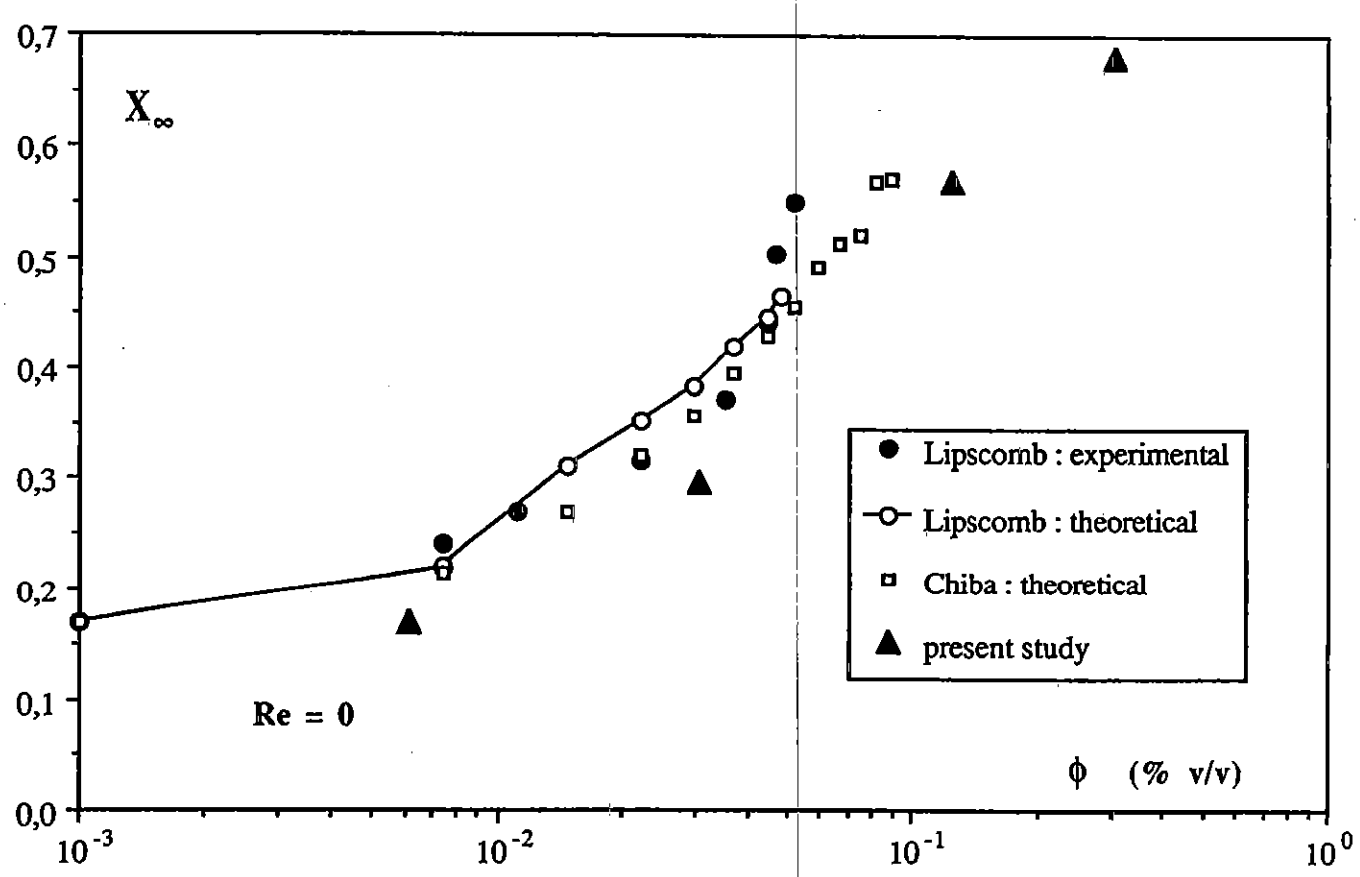

Figure 3.13 : Influence of the concentration on the final non-dimensionalized vortex length. Comparison with other studies.

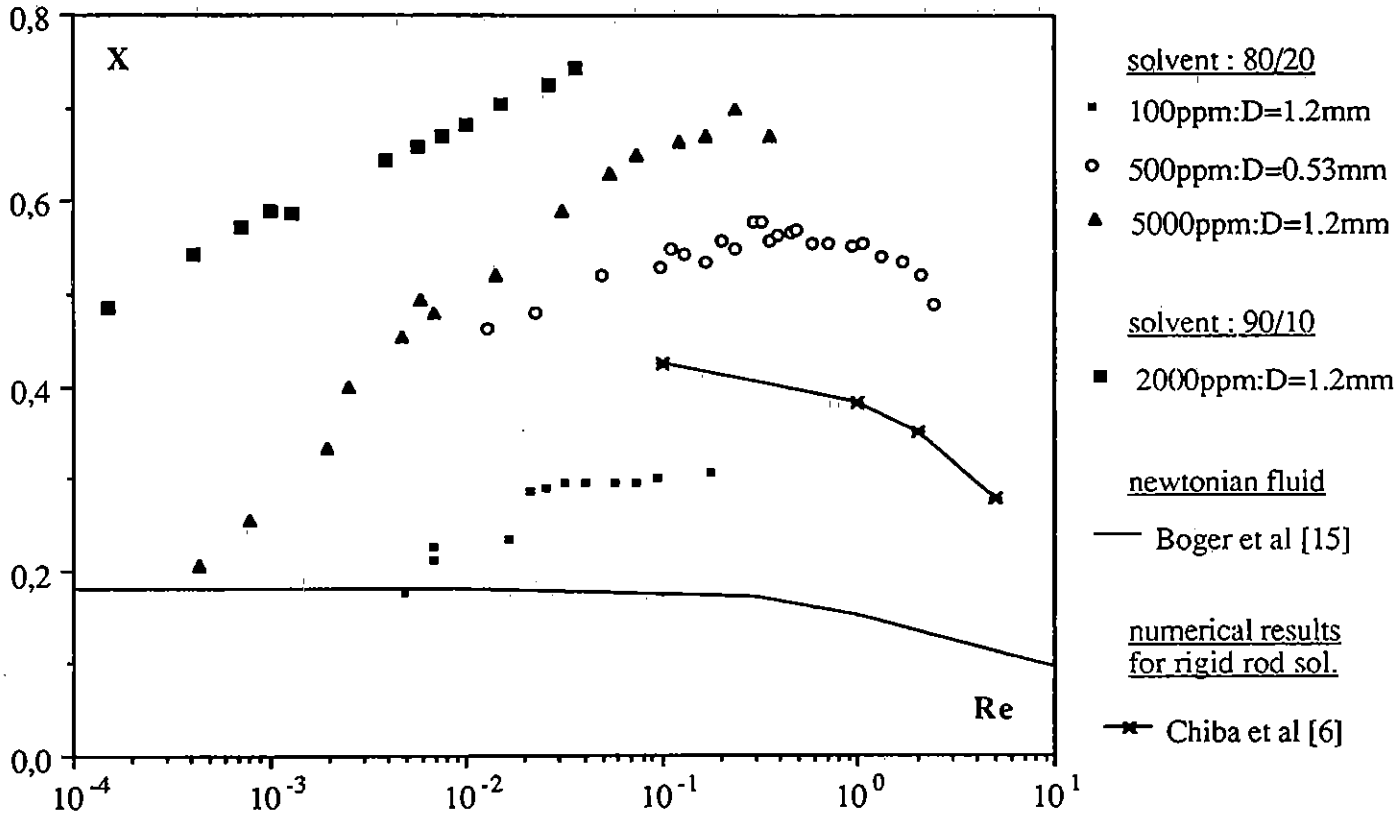

Figure 3.14 : Reduced vortex height versus Re

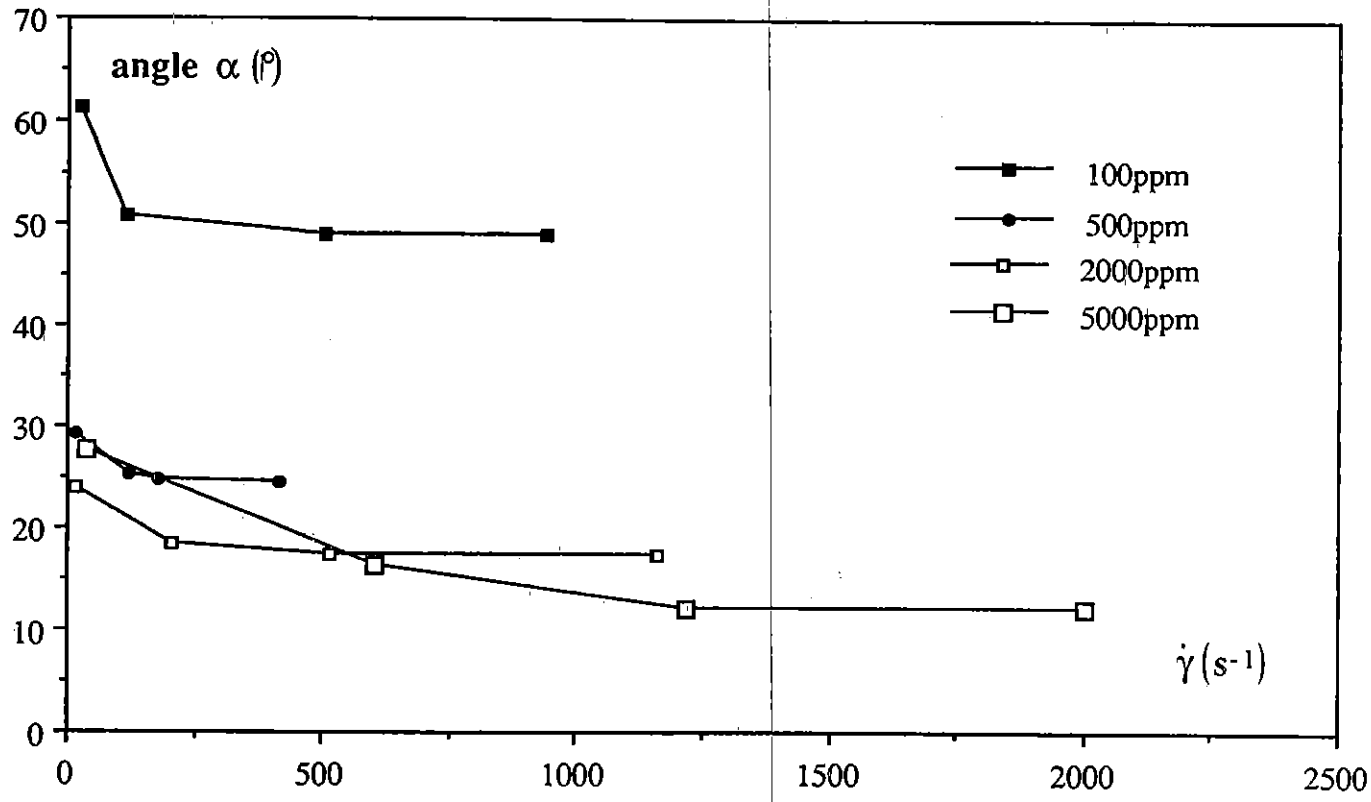

Figure 3.15 : Evolution of the entrance angle for the scleroglucane solutions

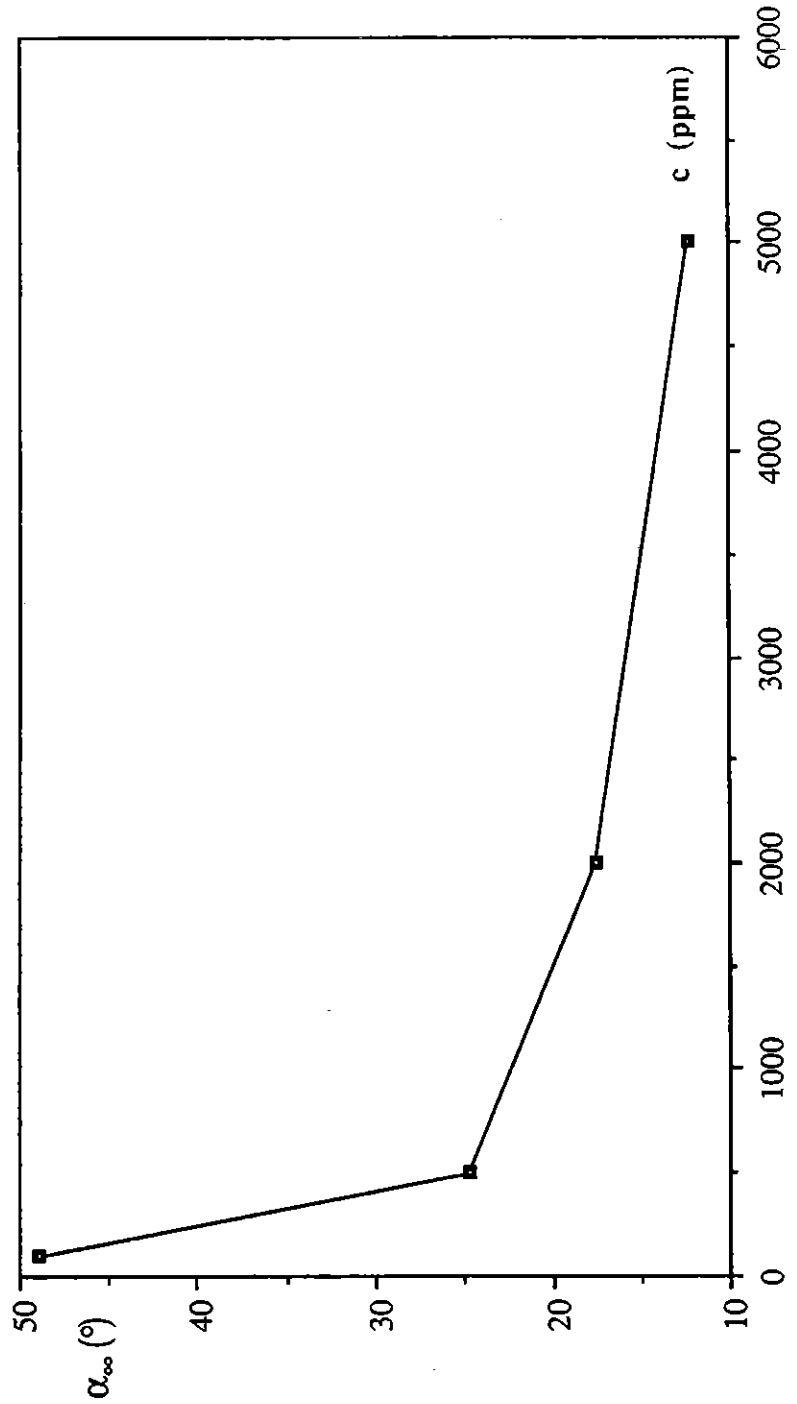

Figure 3.16 : Evolution of the final entrance angle with concentration

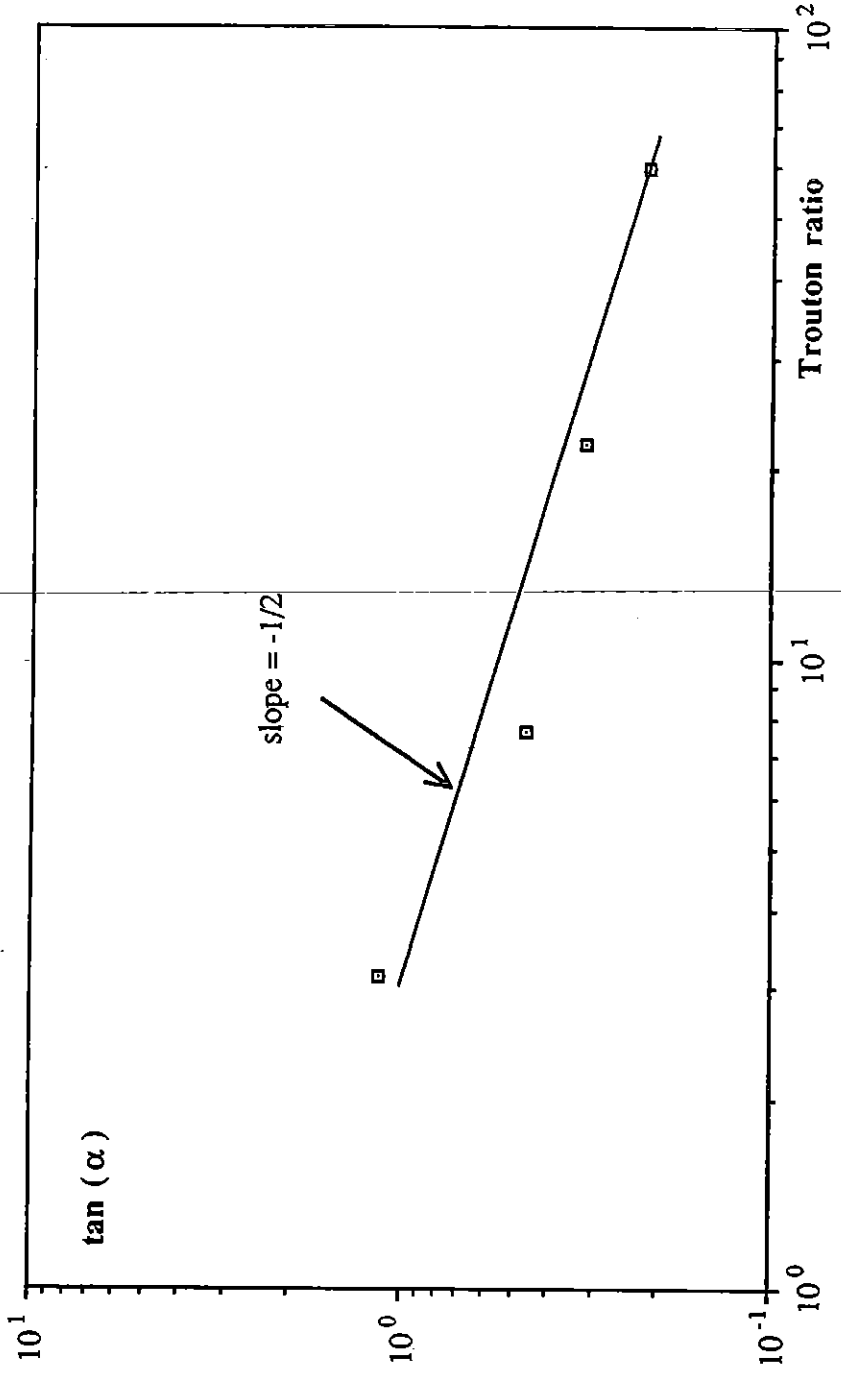

Figure 3.17 : Evolution of the vortex angle with Trouton ratio

Table 3.8 : The flow curves of the scleroglucane solutions in the 80/20 syrup (d=1,2 mm).

100 ppm		500 ppm		5000 ppm	
$q_v\left(\frac{mm^3}{s}\right)$	P_g (mbar)	$q_v\left(\frac{mm^3}{s}\right)$	P_g (mbar)	$q_v\left(\frac{mm^3}{s}\right)$	P_g (mbar)
4,482	0,883	2,443	0,988	1,641	1,675
5,012	0,999	3,560	1,321	2,749	2,883
5,535	1,029	6,061	2,395	6,020	6,188
6,275	1,156	12,659	4,923	7,446	7,499
6,321	1,252	16,122	6,052	12,719	12,900
7,932	1,612	20,697	8,162	15,279	15,977
9,643	1,929	23,284	9,196	17,625	18,352
11,420	2,284	29,956	11,404	32,454	32,443
15,037	2,992	49,536	19,684	63,166	68,588
19,363	3,944	70,679	28,152	102,429	90,618
23,249	4,896	99,265	39,439	134,564	124,879
29,261	6,392	130,719	51,507	206,972	186,486
36,863	8,432	635,674	237,125	266,938	214,528
52,521	12,121			362,077	296,273
67,873	16,322				
85,973	20,452				
159,477	38,832				

Table 3.9: The flow curves of the scleroglucane solutions (end).

2000 ppm in 90/10 syrup (d=1.2 mm)		500 ppm in 80/20 syrup (d=0.53 mm)			
$q_v\left(\frac{mm^3}{s}\right)$	P_g (mbar)	$q_v\left(\frac{mm^3}{s}\right)$	P_g (mbar)	$q_v\left(\frac{mm^3}{s}\right)$	P_g (mbar)
1,14	3,04	6,05	25,0	167,21	675,0
2,94	7,88	10,52	45,0	189,95	780,0
4,95	13,37	22,22	85,0	206,58	875,0
6,96	18,54	43,57	170,0	246,42	975,0
8,61	23,18	49,67	185,0	294,12	1175,0
24,67	67,03	57,56	230,0	383,31	1475,0
34,41	98,28	72,98	300,0	441,18	1675,0
45,55	125,96	87,01	355,0	537,82	1980,0
59,62	165,71	100,69	400,0	688,45	2475,0
87,32	227,86	127,45	480,0	841,63	2975,0
145,27	383,02	135,95	520,0	995,48	3475,0
197,00	552,09	149,02	615,0		

Table 3.10 The shear viscosity of the 100ppm solution of scleroglucan in glucose/water at four different temperatures.

T = 20 °C		T = 17 °C		T = 23 °C		T = 26 °C	
$\dot{\gamma}(s^{-1})$	η (Pa.s)	$\dot{\gamma}(s^{-1})$	η (Pa.s)	$\dot{\gamma}(s^{-1})$	η (Pa.s)	$\dot{\gamma}(s^{-1})$	η (Pa.s)
0,65	1,34	0,42	1,85	5,77	1,04	5,03	0,82
9,28	1,29	4,09	1,83	12,12	1,04	17,35	0,83
15,04	1,31	7,85	1,82	17,80	1,04	33,79	0,82
21,35	1,28	11,51	1,82	23,42	1,04	67,05	0,82
33,53	1,27	15,20	1,82	29,17	1,03	83,90	0,81
45,80	1,27	19,05	1,80	34,88	1,03	100,50	0,81
57,95	1,27	22,43	1,83	40,70	1,03	117,50	0,81
63,31	1,28	26,47	1,80	45,85	1,04	123,90	0,81
76,06	1,28	30,28	1,79	51,56	1,04		
88,34	1,28	33,55	1,82	57,43	1,03		
100,20	1,28	37,69	1,79	63,45	1,02		
111,40	1,29	41,34	1,79	71,12	1,03		
		45,33	1,78	77,09	1,03		
		48,61	1,80	82,26	1,03		
		52,20	1,80	88,56	1,03		
		55,84	1,79	94,01	1,03		

Table 3.11 The shear viscosity of scleroglucan in the glucose/water solvent solutions at 20°C.

c = 500ppm (solv. : 80/20)		c=2000ppm (solv. : 90/10)		c = 5000ppm (solv. : 80/20)	
$\dot{\gamma}(s^{-1})$	η (Pa.s)	$\dot{\gamma}(s^{-1})$	η (Pa.s)	$\dot{\gamma}(s^{-1})$	η (Pa.s)
0,30	1,89	0,006	19,51	0,01	15,54
0,40	1,90	0,017	19,54	0,06	13,19
1,60	1,79	0,081	18,49	0,21	10,68
3,08	1,75	0,120	18,81	1,72	7,43
4,63	1,69	0,168	17,26	3,79	6,36
7,17	1,71	0,292	16,82	5,83	5,95
12,52	1,66	0,814	15,75	7,49	5,73
18,73	1,64	1,673	14,87	9,52	5,54
22,25	1,65	2,572	14,36	11,80	5,30
31,35	1,64	3,558	14,20	13,49	5,37
35,67	1,64	3,884	13,97	15,38	5,24
42,34	1,63	4,640	13,64	17,23	5,16
47,77	1,62	5,471	13,50	19,23	5,06
55,31	1,62	6,227	13,56	21,10	5,07
59,53	1,62	7,304	13,42	23,25	5,03
62,51	1,60	8,192	13,25	25,57	4,92
70,79	1,62	8,880	13,24	27,71	4,95
83,45	1,62	9,287	13,39	29,77	4,91
97,50	1,60	9,533	13,36	30,41	4,93
99,21	1,61	11,270	13,31		
102,90	1,60				

Table 3.12 The shear viscosity of the aqueous scleroglucan solutions at 20°C.

1%		0,1%		1% : creep test		0,1% : creep test	
$\dot{\gamma}(s^{-1})$	η (Pa.s)	$\dot{\gamma}(s^{-1})$	η (Pa.s)	$\dot{\gamma}(s^{-1})$	η (Pa.s)	$\dot{\gamma}(s^{-1})$	η (Pa.s)
0,01	1202,00	0,03	1,7390	0,00003	8780,5	0,00020	25,634
0,01	614,00	0,06	1,3900	0,00015	3957,7	0,00024	29,302
0,03	222,20	1,25	0,2430	0,00022	4545,5	0,00060	16,538
0,04	195,50	2,92	0,1230	0,00055	3662,0	0,00099	10,108
0,05	159,80	9,37	0,0538	0,01397	429,5	0,00139	14,348
0,07	116,10	29,36	0,0240	0,26042	38,4	0,00253	11,860
0,10	91,33	70,88	0,0126			0,00788	6,344
0,12	78,53	93,96	0,0106			0,02438	3,281
0,13	73,99	144,50	0,0091			0,03032	3,298
0,15	66,80	204,80	0,0076				
0,38	34,93	399,00	0,0057				
1,38	13,35	607,60	0,0048				
1,57	12,10	794,70	0,0046				
9,68	2,48	931,90	0,0041				
31,50	0,80	1123,00	0,0038				
90,52	0,28	1222,00	0,0037				
194,00	0,13	1318,00	0,0037				
761,70	0,04	1442,00	0,0036				
1417,00	0,03	1665,00	0,0034				
1840,00	0,02	2015,00	0,0032				
2402,00	0,02	2218,00	0,0032				
		2516,00	0,0034				
		2567,00	0,0031				